



ANFIS Controlled MMC-UPQC to Mitigate Power Quality Problems in Solar PV Integrated Power System

Rajesh Garikapati^{1,*}, S. Ramesh Kumar¹, N. Karthik²

¹ Department of Electrical Engineering, Annamalai University, Tamil Nadu, India

² EEE Department, Bapatla Engineering College, Andhrapradesh, India

ARTICLE INFO

Article history:

Received 17 September 2023

Received in revised form 6 October 2023

Accepted 1 December 2023

Available online 25 December 2023

Keywords:

Solar integration; Power quality challenges; ANFIS controlled MMC UPQC; Voltage fluctuations; Harmonics mitigation; Reactive power compensation; DC link voltage regulation; Grid stability

ABSTRACT

This paper focuses on the implementation of a Modular Multilevel Converter (MMC) based Unified Power Quality Conditioner (UPQC) in a grid-integrated Photovoltaic (PV) system. The integration of photovoltaic (PV) systems into the grid brings numerous benefits in terms of renewable energy utilization like sustainable energy generation, energy security, grid resilience, and economic growth. However, the voltage source converters (VSCs) employed in PV systems can introduce power quality (PQ) issues, including voltage fluctuations, harmonics, and reactive power imbalances and grid instability. The objective of this work is to enhance power quality by mitigating voltage and current fluctuations and harmonics generated due to VSC, compensating reactive power requirements by the load and PV system, and regulating the DC link voltage. For DC voltage regulation, an Adaptive Neuro-Fuzzy Inference System (ANFIS) controller is employed to control for MMC-UPQC. The proposed control strategy is simulated using MATLAB/SIMULINK software and the results are compared with conventional Proportional Integral (PI) and fuzzy controllers. Various dynamic conditions such as voltage sag and swell at the point of common coupling (PCC), changes in irradiance for the PV system, and load variations are considered. The simulation results demonstrate that the ANFIS-controlled MMC-based UPQC outperforms the PI and fuzzy controllers in terms of power quality improvement. It effectively suppresses harmonics, maintains a stable DC link voltage, and compensates for reactive power fluctuations. The proposed control strategy provides superior performance and achieves better power quality compared to conventional controllers. The findings of this work highlight the potential of using an ANFIS controller in MMC-based UPQC systems for grid-integrated PV systems.

1. Introduction

Maintaining satisfactory levels of electrical power quality has posed an ongoing difficulty in distribution systems [1]. Inadequate power quality can lead to various negative consequences, impacting both the electrical system and the connected equipment [2]. In general, below-par power

* Corresponding author.

E-mail address: rajeshgarikapati@gmail.com

<https://doi.org/10.37934/araset.36.1.102130>

quality can result in various problems, including a rise in power wastage, poor performance of the devices, and disruption of nearby communication systems, among other detrimental effects.

A unified power quality conditioner (UPQC) to fix the power quality issues. The UPQC design is linked to the three-phase, four-wire infrastructure. The fourth wire of the system contains the series transformer's neutral. The use of a four-leg voltage source inverter design for the shunt section mitigates any neutral current that may flow towards the neutral point of the transformer. Under all operational conditions, the series transformer neutral will have a potential of virtually zero. In this, a nonlinear load and a linear load are combined with a united power quality conditioner to examine power quality issues such as harmonics, imbalanced voltage, and current. Additionally, the THD (1.46%), active power, and reactive power were calculated.

1.1 Need of Power Quality In UPQC

In UPQC, two significant types of APF are shunt APF and series APF, as stated in [5,6]. The shunt APF is the most effective in addressing current-related issues, while the series APF is the most appropriate for mitigating voltage-related problems. As the current distribution system necessitates a higher-quality voltage supply and current draw, the installation of APFs has immense potential for actual practical implementation [7,10]. A reduction in RMS voltage or current for periods ranging from 0.5 cycles to 1 minute is known as a sag. A brief, 0.5–1 minute, rise in the RMS value of the voltage or current. Fluctuations or flickers in the voltage Changes in voltage are comparatively minor variations in the RMS line voltage (less than 5%). The principal causes of these changes in speed include cycle converters, arc furnaces, and other equipment that demands current that is not synchronised with the line frequencies [11].

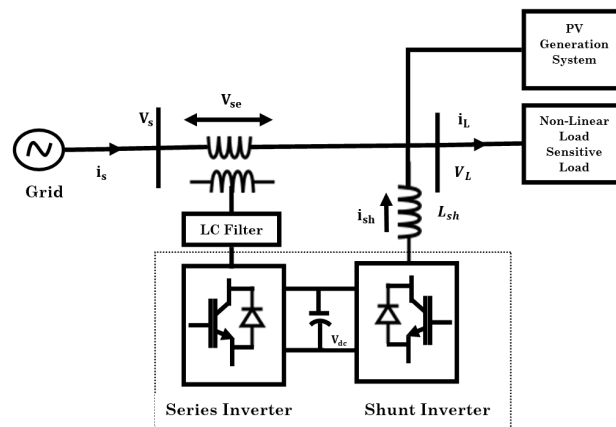


Fig. 1. UPQC general block diagram representation

A UPQC shares similarities with a unified power flow controller (UPFC) in terms of its construction [12]. Power quality, which refers to all factors affecting the magnitude, phase, and inverse time of the analogous voltage and current in a power circuit, for instance, is a crucial concept. Power quality impurities are any issue coherent in voltage, current, or inverse time variation that causes Failure of the client equipment. The quality of the supply of electrical power has been significantly impacted by the growing use of power electronics-based devices. The generation of electricity, damage to machinery or appliances, increased power losses, interference with the transmission of information, and other issues can be impacted by the quality of the electric grid. It follows that maintaining a high standard for power quality is reasonable.

The aim of a UPQC is to mitigate issues related to power quality in the supply voltage, such as sags, swells, unbalance, flicker, and harmonics, as well as problems in load current quality, such as harmonics, unbalance, reactive current, and neutral current. The system configuration of UPQC is represented by a single-line diagram, as shown in Figure 1. The essential components of this system are:

- i. The UPQC system configuration includes two inverters, one connected in parallel with the load, which functions as a shunt APF, and the other connected in series with the line, acting as a series APF.
- ii. The shunt coupling inductor L_{sh} is utilized to connect the shunt inverter to the network and to smooth the current waveform. In some cases, an isolation transformer is used to isolate the inverter from the network.
- iii. In Figure 1, a capacitor is utilized to form a common dc link between the two inverters. This capacitor not only interconnects the two inverters but also ensures a constant self-supporting dc bus voltage across it.
- iv. An LC filter is used as a passive low-pass filter (LPF) to remove high-frequency switching ripples from the generated inverter output voltage.
- v. A series injection transformer is employed to interface the series inverter with the network. To reduce the current or voltage rating of the series inverter, a suitable turn ratio is often used.

The UPQC is essentially a combination of shunt and series APFs that share a self-supporting dc bus. The shunt inverter in the UPQC is operated in current control mode and delivers a current equal to the reference current set by the UPQC control algorithm. The shunt inverter is also responsible for maintaining a stable DC bus voltage at a set reference value, to achieve the required performance from a UPQC system. The shunt inverter should inject a current according to the Eq. (1) to cancel the harmonics generated by a nonlinear load:

$$i_{sh}(\omega t) = i_s^*(\omega t) - i_L(\omega t) \quad (1)$$

The Eq. (1) represents the relationship between the shunt inverter current, reference source current, and load current. The shunt inverter current, denoted as $i_{sh}(\omega t)$, should be equal to the difference between the reference source current, denoted as $i_s^*(\omega t)$, and the load current, denoted as $i_L(\omega t)$, multiplied by a harmonic cancellation factor. The purpose of this Eq. (1) is to cancel out the harmonics generated by a nonlinear load by injecting a compensating current. The series inverter of UPQC is controlled in voltage control mode to generate a voltage and inject it in series with the line to achieve a sinusoidal, distortion-free, and desired magnitude voltage at the load terminal. The basic operation of the series inverter can be represented by the Eq. (2):

$$v_{sr}(\omega t) = v_L^*(\omega t) - V_S(\omega t) \quad (2)$$

$v_{sr}(\omega t)$ is the injected voltage by the series inverter, $v_L^*(\omega t)$ is the reference load voltage, and $V_S(\omega t)$ is the actual source voltage, respectively. When there is a voltage sag condition, V_{sr} will represent the difference between the reference load voltage and the reduced supply voltage, i.e., the voltage injected by the series inverter to maintain the load terminal voltage at the reference value [13].

Grid-integrated Photovoltaic (PV) systems play a significant role in renewable energy generation and have gained substantial attention in recent years. However, the fluctuating nature of solar power and the presence of nonlinear loads can lead to power quality issues, including voltage and current harmonics. To address these challenges, the MMC based UPQC has emerged as a promising solution. This paper presents the implementation of an ANFIS-controlled MMC-based UPQC in a grid-integrated PV system. The objective is to enhance power quality by effectively filtering out harmonics caused by the Voltage Source Converter (VSC) of the PV system and maintaining a stable grid operation. The ANFIS controller, which utilizes adaptive neuro-fuzzy inference systems, offers improved control capabilities compared to conventional PI and fuzzy controllers. Through simulations conducted using MATLAB/SIMULINK software, the proposed ANFIS-controlled MMC-based UPQC is evaluated and compared with PI and fuzzy controllers. Various dynamic conditions, including voltage sag and swell, changes in irradiance, and load variations, are considered to assess the performance of the system.

2. Modular Multilevel Converter Control Technique

The MMC presents several attractive topologies and has versatile applications. In situations where high voltages are involved, MMC can eliminate the need for a single DC source and transformer. To generate a high-quality multilevel voltage waveform, the submodules of MMC are connected in a series configuration to achieve the system voltage. These submodules are composed of IGBTs, diodes, and capacitors and can take various shapes and forms. The number of submodules needed to design MMC depends on factors such as the application, the operating voltage, and the IGBT rating.

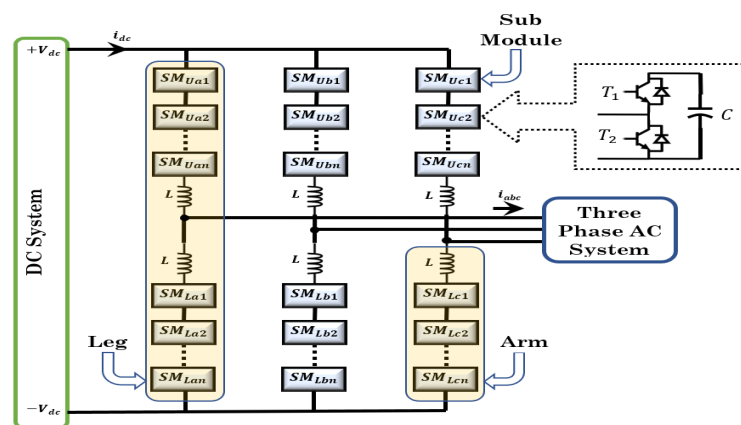


Fig. 2. Structure of MMC

Figure 2 illustrates a three-phase MMC that performs the DC to AC conversion. In this configuration, the positive and negative terminals of the three legs are connected to the DC link, while the midpoint of each leg is connected to a three-phase AC system. These midpoints effectively split each leg into two parts, known as the positive arm and the negative arm. Each section of the MMC consists of a current-limiting inductor and series-connected submodules. To prevent the circulating current from increasing with the difference in instantaneous voltages between the arms, an inductor is used as a current-limiting device. The modular design of the MMC allows for the scalability of voltage and power ratings across the submodules. The MMC can convert unidirectional DC voltage into bidirectional stepped voltage with minimal dv/dt ratio, low total harmonic distortion

(THD), and reduced current ripples. The series-connected submodules allow for low switching frequency control and facilitate fault-tolerant operation.

A submodule (SM) is a basic circuit that converts unidirectional voltage to bidirectional voltage using low voltage switching devices. The submodule can be powered by a capacitor, allowing for the application of unidirectional or DC voltage. Several submodule types are commonly utilized in MMC, including Half-bridge (HB), Full-bridge (FB), flying capacitor (FC), Cascaded half-bridge (CH), and Double clamp (CD) submodules. Figure 2 illustrates the configuration of a half-bridge submodule, which consists of two IGBTs, two anti-parallel diodes, and a capacitance. The submodule operates using the complementary action of the two IGBT switches, T_1 and T_2 , which alternately turn on and off to regulate the voltage of the DC capacitor, v_c . When one switch is on, the other is off, and vice versa.

When the T_1 switch of the submodule on the DC side is turned on, the capacitor current, i_c , is equal to the submodule current, i_{sub} . When the switch is turned off, the capacitor current is 0. Figure 3 illustrates that there are two possible energy points at the AC side of the submodule, which can be either v_{dc} or 0. When the T_1 switch is turned on, the voltage at the AC side of the submodule v_{sub} , is equal to the capacitor voltage, v_c .

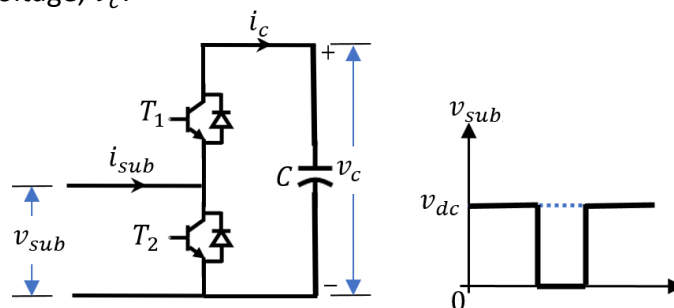


Fig. 3. Switching states of MMC

The voltage of the DC capacitor, v_c , can be expressed in terms of the current through the capacitor as shown in Eq. (3) and Eq. (4)

$$v_c = \frac{1}{C} \int_0^t i_c(\tau) d\tau \quad (3)$$

$$i_c(\tau) = T_1 i_{sub} \quad (4)$$

The capacitor voltage increases when the capacitor current i_c , flows in a positive direction, whereas it decreases when i_c flows in a negative direction. When T_1 is turned off, the AC side voltage v_{sub} , becomes zero, and the capacitor voltage, v_c , remains constant. The switching states of the half-bridge submodule are summarized in the Table 1.

Table 1
 Changing States of half-bridge switching module

Switching State S	T_1	T_2	v_{sub}	$i_{sub} > 0$	$i_{sub} < 0$
1	ON	OFF	v_c	v_c increases	v_c decreases
0	OFF	ON	0	v_c constant	v_c constant

MMC converts a constant DC voltage into a bidirectional multilevel stepped voltage waveform by using series-connected submodules that are constructed in a similar manner. The number of stages that can be achieved depends on the total number of cascaded submodules that are connected in each leg of the arm. If 'n' submodules are connected in each leg with a rated capacitor voltage of v_c ,

then the output voltage from the submodules can be denoted as $v_{sub1}, v_{sub2}, v_{sub3}, \dots, v_{subn}$. With 'n' number of submodules, 'n+1' voltage levels can be achieved, which are $0, v_c, 2v_c, 3v_c, \dots, nv_c$. It is possible to achieve a voltage level of 0 by turning off all submodule switches. By combining different switching states of submodules, other voltage levels can be generated. The switching states control and regulate the capacitor voltage of each submodule, and the output voltage of each arm of the MMC, denoted as v_{arm} is equal to the sum of voltages of each submodule as shown in Eq. (5).

$$v_{arm} = v_{sub1} + v_{sub2} + v_{sub3} \dots + v_{subn} = S_1 v_{c1} + S_2 v_{c2} + S_3 v_{c3} + \dots S_n v_{cn} \quad (5)$$

$S_1, S_2, S_3, \dots, S_n$ are switching states (either 1 or 0) of submodules.

3. UPQC in Grid Integrated PV Control Methodology

3.1 System Description

The system depicted in Figure 4 consists of a nonlinear load, a series converter, a shunt converter, and a PV generation system. The DC link voltage, denoted as v_{dc} , represents the voltage across both the series and shunt converters. The system also includes various voltage and current parameters, such as v_{gabc} and i_{gabc} (source voltage and current), R_g and L_g (line resistance and inductance), v_{ca}, v_{cb} and v_{cc} (series converter injected voltages through a series transformer), i_{cabc} (compensator current injected by the shunt converter), v_{labc} and i_{labc} (load voltage and current), and i_{pvabc} (PV injected current).

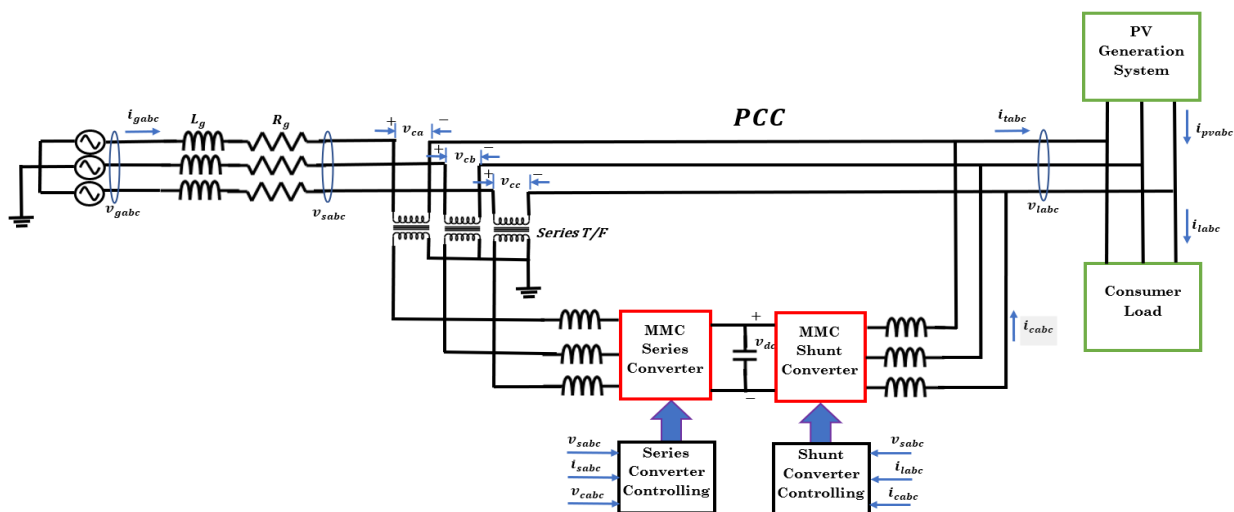


Fig. 4. PV Integrated power system with MMC-UPQC

Figure 5 illustrates the PV generation system comprising an MPPT-operated DC-DC converter and a voltage source converter (PV-VSC). The purpose of the MPPT-operated DC-DC converter is to efficiently convert the voltage and current from a PV source to a different voltage level while optimizing power transfer. It achieves this through the implementation of MPPT technology, which enables the extraction of maximum available power from a DC power source like a solar panel. By continuously monitoring the power source's output, the converter adjusts its operating point to match the maximum power point (MPP) of the source. The MPP refers to the combination of voltage and current at which the power output is maximized. The MPPT technique employed in this paper is incremental conductance-based MPPT (INC-MPPT). This approach relies on the principle that the derivative of the power-voltage curve of a solar panel is zero at the MPP. By measuring the voltage

and current of the solar panel, the INC-MPPT algorithm determines the direction in which the operating point should be adjusted to reach the MPP. Compared to other MPPT techniques, INC-MPPT offers faster and more accurate tracking of the maximum power point. It swiftly adapts the operating point in response to variations in solar irradiance, temperature, and other factors, ensuring optimal efficiency of the solar panel.

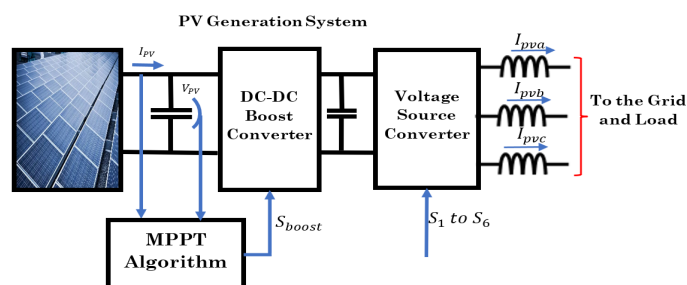


Fig. 5. PV Generation System

The voltage source converter (VSC) plays a crucial role in photovoltaic (PV) generation systems as it converts the DC power produced by solar panels into AC power suitable for connection to the utility grid or for local usage. By providing control over the output voltage and frequency, the VSC enables the PV system to operate independently or in coordination with the grid. However, the operation of VSCs, which involves rapidly switching power semiconductor devices like insulated gate bipolar transistors (IGBTs), can introduce harmonics into the power grid. These harmonics arise from the rapid on-off switching actions employed to generate the desired voltage and current waveforms. To synthesize the desired output voltage waveform, VSCs often utilize pulse width modulation (PWM) techniques. PWM involves generating voltage pulses with adjustable widths to approximate a sinusoidal waveform. Nevertheless, the quick switching of these pulses can introduce harmonics due to the abrupt changes in voltage and current. Furthermore, the switching frequency of VSCs can contribute to harmonic injection. While higher switching frequencies allow for improved approximation of the waveform, they can also lead to a higher level of harmonic content due to the increased number of switching instances. VSCs are commonly employed as interfaces for nonlinear loads, such as electronic equipment and variable speed drives. These nonlinear loads draw non-sinusoidal currents, which can further exacerbate harmonic distortion and complicate power quality issues.

3.2 Unified Power Quality Conditioner with MMC

The series active filter (SeAF) and shunt Harmonic Active Power Filter (HAPF) of UPQC consist of a MMC with 8 submodules in each leg, resulting in a total of 4 submodules for the positive arm and 4 submodules for the negative arm. Each submodule utilizes a half bridge configuration that includes two insulated gate bipolar transistors (IGBTs), two anti-parallel diodes, and a DC capacitor. The switching states of these submodules are elaborated upon in Section II. Figure 4 illustrates the proposed model aimed at enhancing power quality through the utilization of an MMC-based UPQC.

The initial step in the design of an MMC-UPQC for a PV-grid integrated system involves determining suitable sizes for key components such as the PV array, DC-link capacitor, and DC-link voltage level. It is essential to correctly size both the shunt compensator and series compensator to handle the peak power output from the PV array and grid, as well as to effectively compensate for reactive power and current harmonics associated with the load current. The PV array's sizing is critical as it needs to match the AC grid voltage at its maximum power point (MPP) voltage to establish a

connection with the grid through the MMC-UPQC. Under normal operating conditions, the PV array should be capable of providing the required active power for the load while also supplying power to the grid. Detailed specifications for various design components, including the PV array and other elements such as interfacing inductors for the series and shunt compensators, as well as a series injection transformer for the series compensator, are outlined in Table 2.

The recommended approach for managing the MMC-UPQC system involves employing the Synchronous Reference Frame (SRF) technique, which allows for independent control of the shunt Harmonic Active Power Filter (HAPF) and the series Active Power Filter (APF). The shunt HAPF utilizes a dual-loop feedback method and a voltage feedforward mechanism to counteract harmonic currents and maintain the stability of the DC-link voltage. On the other hand, the series APF employs a voltage feedback mechanism and a current feedforward approach to regulate the distorted load voltage. To ensure the synchronization of both the series and shunt HAPF with the grid, a control system capable of handling non-ideal grid voltage conditions is required. Traditional Synchronous Reference Frame Phase-Locked Loop (SRF-PLL) systems often exhibit poor performance under such conditions. To address this issue, this paper proposes the adoption of a pre-sorting SRF-PLL approach based on the Sliding-Mode Generalized Discrete Fourier Transform (SGDFT) technique. By incorporating the SGDFT-pre-filter, the SRF-PLL can effectively operate even in the presence of significantly abnormal grid voltage conditions, provided that the Proportional Integral (PI) benefits are appropriately tuned. This approach enhances the stability and performance of the MMC-UPQC system, allowing for effective control and mitigation of power quality issues in the grid-connected environment.

3.3 Control Strategy for ShAF

The control block diagram of the shunt Harmonic Active Power Filter (HAPF) is presented in Figure 6. This diagram consists of various modules, including reference current calculation, DC-link voltage control, output current control, voltage feedforward control, and Carrier-Based Sinusoidal Pulse Width Modulation (SPWM). To determine the reference current, SGDFT is employed on the load current. The SGDFT method analyses the load current waveform and calculates the desired reference current for the HAPF. The DC-link voltage control module utilizes a fuzzy device to normalize the DC-link voltage and ensure it matches the desired value, denoted as v_{dc}^* . This normalization process involves generating a reactive current, referred to as i_q . Additionally, the active current, i_d , is assumed to be zero. The Park transformation is then applied to convert the dq terms into abc coordinates, resulting in (i_{2abc}) representation.

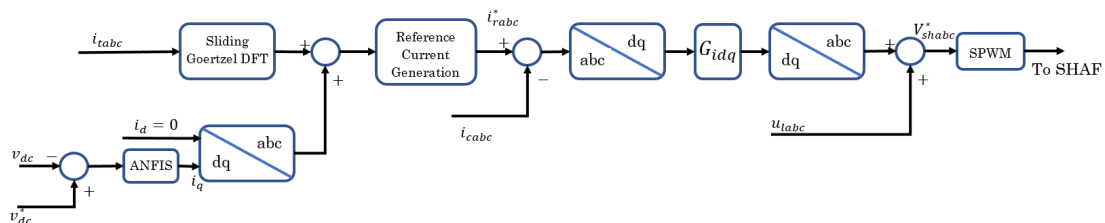


Fig. 6. Control structure of shunt active power filter

Then reference currents can be calculated from the Eq. (6)

$$i_{rabc}^* = i_{2abc} + i_{tabc} \tag{6}$$

The goal is to design a Proportional Resonant (PR) controller that follows the current reference. The transmission work of the switch in the distinct domain can be obtained using the impulse invariant method [14], which is expressed as given in Eq. (7):

$$G_{idq} = K_{pi} + \sum_{h=6,12} \frac{2K_{ii}T_s(1-z^{-1} \cos(\omega_h T_s))}{1-2z^{-1} \cos(\omega_h T_s)+z^{-2}} \quad (7)$$

Wherever K_{pi} is related constant, K_{ii} is fundamental constant, T_s is the sample interval,

To mitigate the impact of the dominant harmonic orders (specifically the 5th, 7th, 11th, and 13th harmonics) present in the load current, the control system incorporates Proportional Resonant (PR) controllers in the DQ domain. These PR controllers are designed specifically for the 6th and 12th harmonic orders to effectively suppress them and reduce their influence on the system. Furthermore, to compensate for any disturbances or disruptions in the grid voltage, a voltage feed-forward control approach is implemented. This control strategy anticipates changes in the grid voltage and takes proactive measures to counteract them, ensuring a stable and reliable operation of the system. To generate the necessary pulses for the MMC employed in the SeAF, a sinusoidal pulse width modulation (SPWM) technique is utilized. This modulation technique enables the precise generation of pulses that correspond to the desired output waveform, allowing for effective compensation and harmonic mitigation by the SeAF.

3.4 Control Strategy for SeAF

Figure 7 illustrates the control architecture employed in the SeAF. This architecture comprises several components, including reference voltage calculation, output voltage control, current feedforward control, and sinusoidal pulse width modulation (SPWM). The reference voltages for the SeAF are generated by considering both the grid voltages (v_{sabc}) and the desired load voltages (v_{labc}^*). The reference load voltages (v_{labc}^*) are derived by considering the fundamental phase sequence and the minimum amplitude of the load phase voltage (v_l^*). Like the current control strategy utilized in the shunt Harmonic Active Power Filter (HAPF), the SeAF incorporates 6th and 12th harmonic Proportional-Resonant (PR) controllers denoted as $G_{vdq}(z)$. These PR controllers play a crucial role in tracking the reference voltages within the sequence active filter. They enable accurate control and compensation of harmonic components by ensuring precise regulation and synchronization with the desired voltage references.

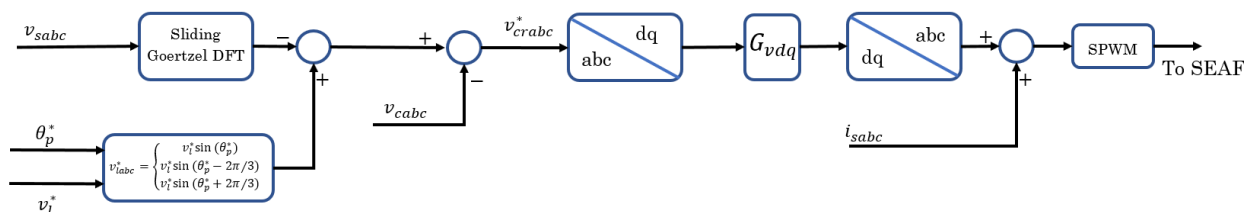


Fig. 7. Control structure of series active power filter

The control architecture integrates current feedforward control and sinusoidal pulse width modulation (SPWM). The current feedforward control plays a crucial role in precise compensation of load current harmonics by incorporating their impact within the control loop. On the other hand, the SPWM technique is employed to generate the necessary pulse patterns that drive the SeAF and enable the generation of desired output voltages. Figure 8 illustrates the control architecture for the

SeAF, encompassing several components, including reference voltage calculation, output voltage control, current feedforward control, and SPWM.

Current feedforward control is employed to compensate for the current disturbances.

$$G_{vdq} = K_{pv} + \sum_{h=6,12} \frac{2K_{iv}T_s(1-z^{-1}\cos(\omega_h T_s))}{1-2z^{-1}\cos(\omega_h T_s)+z^{-2}} \quad (8)$$

Where K_{pi} , K_{ii} , are PI gains and T_s is the sample time.

3.5 Adaptive Neuro Fuzzy Inference System

In this section, a category of adaptive networks known as Neuro-Fuzzy will be presented, along with their corresponding architectures and learning methods. Neuro-Fuzzy systems, which combine Artificial Neural Networks (ANN) with Fuzzy Systems, have a network structure that encompasses all types of neural network paradigms capable of supervised learning. This structure offers the advantage of enabling a straightforward conversion of the resulting system into a set of if-then rules, while also allowing the fuzzy system to be seen as a neural network with distributed knowledge across connection strengths. As its name suggests, an adaptive network is a network architecture that comprises nodes and directional links, and whose overall input-output behaviour is determined by a set of adjustable parameters that connect the nodes [16]. This type of system utilizes a hybrid learning algorithm to identify the parameters of Sugeno-type fuzzy inference systems. The adaptive network applies a combination of the least-squares method and back-propagation gradient descent method to train the membership function parameters of Fuzzy Inference Systems (FIS), which enable it to emulate a provided training data set [16]. The learning process of the network occurs in two primary phases. During the learning algorithm's forward phase, the consequent parameters determine the least squares estimate, while in the backward phase, error signals propagate from the output layer to the input layer. These error signals, which are the derivatives of the squared error with respect to each node output, are used to adjust the network's parameters. During the backward pass, the gradient descent algorithm updates the premise parameters of the network. The learning or training phase of a neural network involves determining parameter values that fit the training data adequately. In ANFIS training, alternative algorithms can be used to minimize the training error. To search for optimal parameters effectively, a combination of the gradient descent algorithm and a least squares algorithm is employed. The primary advantage of utilizing a hybrid approach is that it significantly accelerates convergence by reducing the search space dimensions of backpropagation, which is used in neural networks ANFIS, which is the Sugeno fuzzy model within the framework of an adaptive system, serves to build and validate models and facilitate training and adaptation [17].

3.5.1 Architecture of ANFIS

The parameter set of an adaptive network enables fuzzy systems to learn from the data that they are modelling. In this paper, we examine an adaptive system with two inputs, V1 and V2, and one output, f. We will analyse a first-order Takagi-Sugeno-Kang (TSK) fuzzy inference system that includes two rules.

Rule 1: If (v is V1) and (d is D1) then $f_1 = p_1^v + q_1^d + r_1$

Rule 2: If (v is V2) and (d is D2) then $f_2 = p_2^v + q_2^d + r_2$

The first-order Takagi-Sugeno-Kang (TSK) fuzzy inference system considered in this paper contains two rules, where linear parameters $p_1, p_2, q_1, q_2, r_1,$ and r_2 are used along with non-linear parameters $V_1, V_2, D_1,$ and D_2 . V_1 and D_1 represent the antecedent membership functions of ANFIS, while $p_1, q_1,$ and r_1 are the consequent parameters. We use both circles and squares to represent the adaptive capabilities in the system.

During the design of the ANFIS model, it is crucial to tune the number of training epochs, membership functions, and fuzzy rules accurately. The mapping of these parameters is highly critical for the system because incorrect tuning may lead to overfitting or underfitting of the data. The ANFIS model parameters can be adjusted by using a hybrid algorithm that combines the least-squares method and the gradient descent method with a mean square error method. The aim of this adjustment is to minimize the difference between the ANFIS output and the desired objective, thereby improving the accuracy of the ANFIS system. The training process aims to minimize the training error.

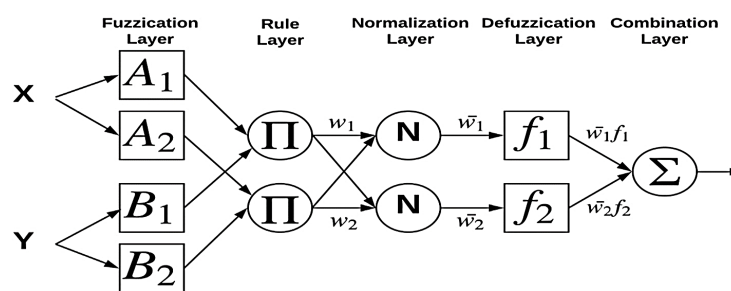


Fig. 8: Basic architecture of ANFIS

3.5.2 ANFIS Design for DC Voltage Regulation in MMC-UPQC

To design an ANFIS in MATLAB to replace PI/Fuzzy controller, following steps are involved based on Figure 9:

- i. Identify the input variables (DC Voltage error and change in error) and the output variable (e.g., control signal). These variables are crucial for the ANFIS controller to learn and make decisions.
- ii. Prepare a set of training data pairs consisting of the input variables and the corresponding desired output (i.e., control signal). The training data should cover a wide range of operating conditions and scenarios.
- iii. Specify the number of membership functions and the type of membership function for each input and output variable. Additionally, determine the number of rules and the type of fuzzy inference system (Sugeno) to be used.
- iv. Use the training data generated in step 2 to train the ANFIS model. The training process adjusts the parameters of the ANFIS model to minimize the error between the model's output and the desired output.
- v. After training, evaluate the performance of the ANFIS model using a separate validation dataset. Adjust the ANFIS parameters or structure if necessary to improve its performance.
- vi. Once the ANFIS model is trained and validated, integrate it into the control system. Replace the Fuzzy/PI controller with the ANFIS model and establish the necessary connections between the ANFIS inputs (e.g., error, change in error) and the ANFIS outputs (e.g., control signal).

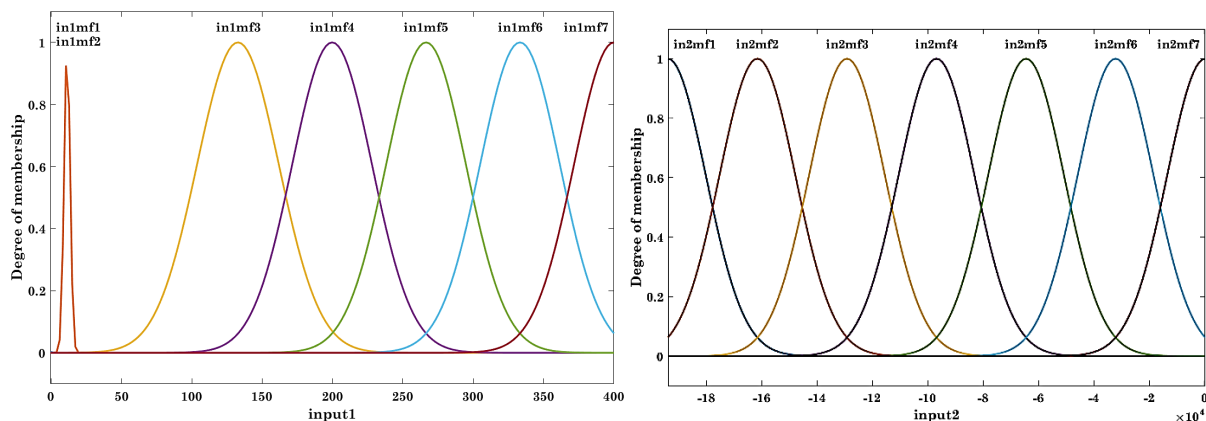


Fig. 9. Input membership functions of ANFIS designed

5. Simulation Results

The objective of this work was to evaluate the performance of an ANFIS controlled MMC-based UPQC through simulations conducted using MATLAB-Simulink. The simulations were carried out considering a grid-connected Photovoltaic (PV) generation system and a three-phase diode bridge rectifier with a nonlinear load. Various dynamic conditions such as voltage sag and swell at the point of common coupling (PCC), changes in PV generation system irradiance, and load variations were simulated. The MATLAB-Simulink software with a solver step size of $1\mu\text{s}$ was used, and the system parameters from Table 2 were utilized. The effectiveness of the ANFIS controlled MMC-UPQC was assessed in terms of harmonic filtering for the nonlinear load and PV generation system's voltage source converter (VSC) to ensure grid power quality. Furthermore, the performance of the ANFIS controlled MMC-UPQC in regulating voltage during point of common coupling(PCC) voltage sag and swell events was evaluated. The simulations were conducted in a 440V distribution network with PV integration, and the results were compared with those obtained from a Proportional Integral (PI) controlled MMC-UPQC and Fuzzy Controlled MMC-UPQC.

Table 2

System Parameters

Parameters	Values
Grid voltage and frequency	440 V, 50 Hz
Line resistance and inductance	0.2 ohm and 0.5 mH
PV generation system	
Open Circuit Voltage	64.2 V
Short Circuit Current	5.96 A
MPP voltage	54.7 V
MPP Current	5.58 A
Parallel Strings	66
Series connected modules per string	5
Series Transformer	630 KVA 440/440 V
Series converter Filter	2mH, 20 μF
Shunt Converter Filter	1.35 mH, 215 μF
MMC	
No. of Sub Modules per leg	8
Capacitance of Sub Module	3.3 mF
DC Link Capacitance	9400 μF

5.1 Case 1: Distorted Source Voltages

In Case 1, the impact of distorted grid voltages on nonlinear loads and a PV system is investigated, and the proposed ANFIS-controlled MMC-UPQC is utilized to mitigate these effects. The grid voltage is deliberately distorted with characteristic harmonics, including the 5th, 7th, 11th, and 13th harmonics, as shown in Figure 10(a). A diode rectifier RL load is connected to the PV-integrated grid system, and the ANFIS-based MMC-UPQC is installed as an intermediary to protect the grid and other consumers from the adverse effects of harmonics generated by the PV system's Voltage Source Converter (VSC) and distortions caused by nonlinear loads.

Figures 10 provide waveforms of the distorted grid voltage, load voltage, and PV system voltage without the ANFIS-based MMC-UPQC. The total harmonic distortion (THD) of these voltages is measured at 11.66%.

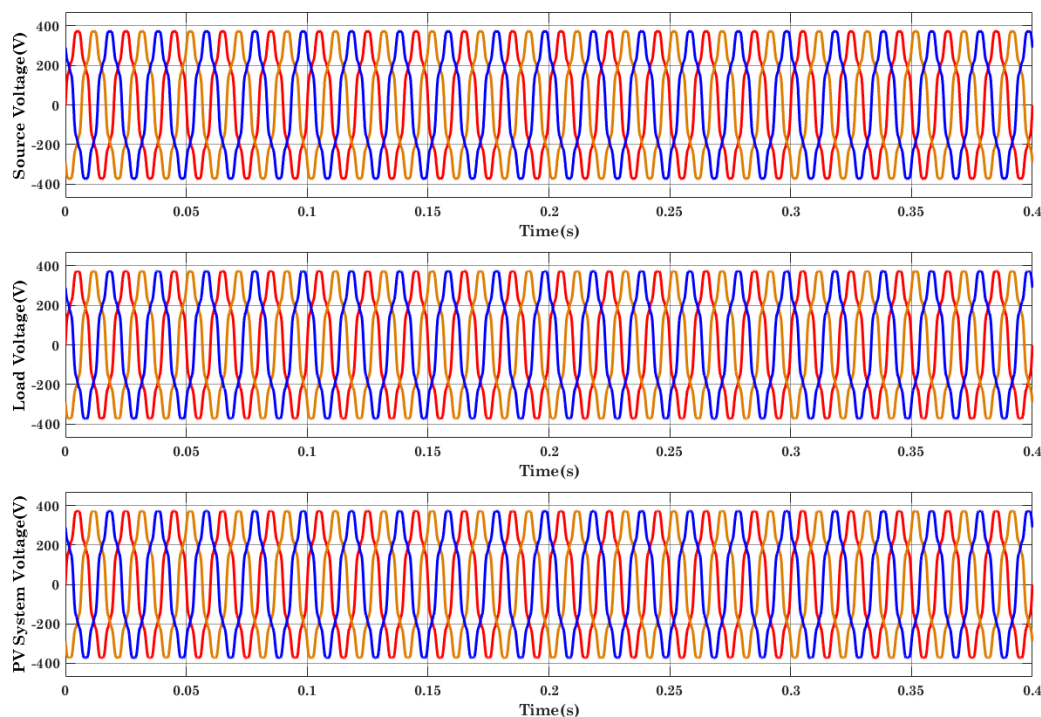


Fig. 10. Source Voltage, Load Voltage, and PV system Voltage without MMC-UPQC

Figure 11 displays the nonlinear load current, source current, and PV system current, all exhibiting significant THD values without the UPQC. The load current has a THD of 30.85%, the source current has a THD of 63.47%, and the PV system current has a THD of 4.95%.

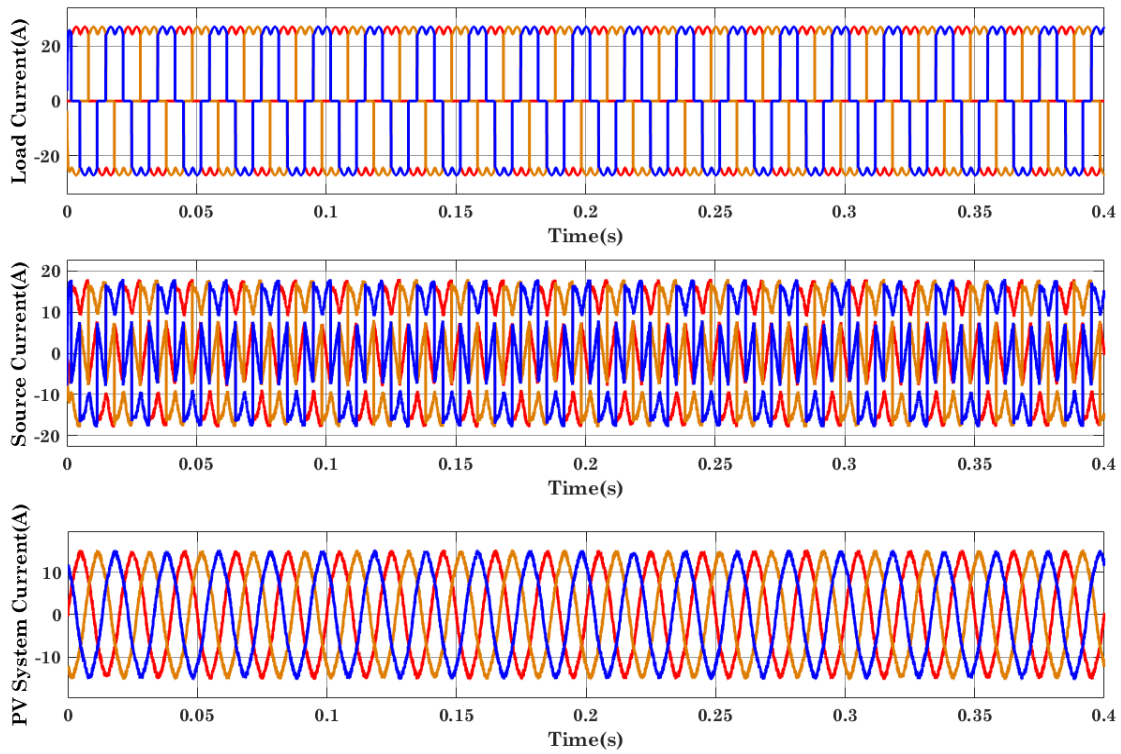


Fig. 11. Non-linear load Current, Source Current and PV system Current without MMC-UPQC

Figure 12 depicts the active power supplied by the grid and PV system to the load. Upon connecting the ANFIS-based MMC-UPQC, the distorted load voltage and source current undergo filtration through the series and shunt converters.

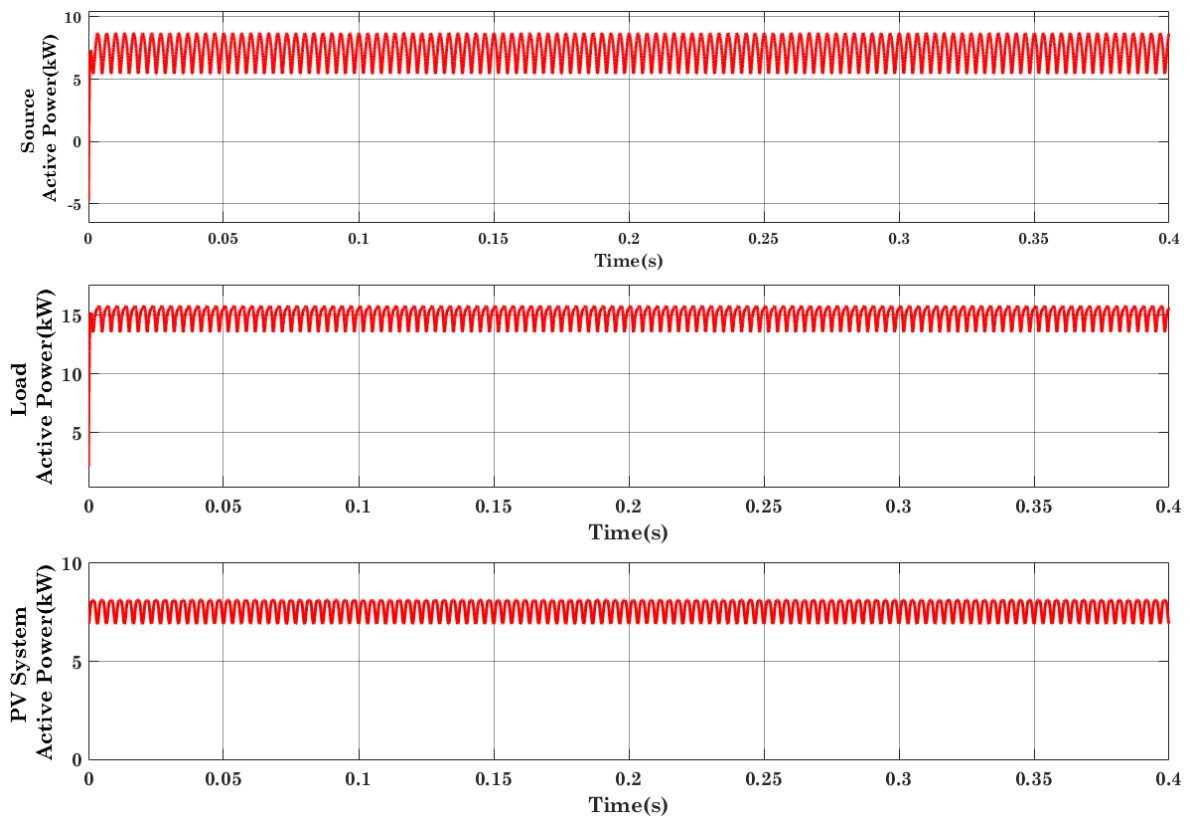


Fig. 12. Instantaneous Active Power at Source, Load and PV System without MMC-UPQC

Figure 13 illustrates the source voltage, load voltage, PV system voltage, and the voltage injected by the series converter. The injected voltage by the series converter significantly reduces the THD of the load voltage to 0.63%.

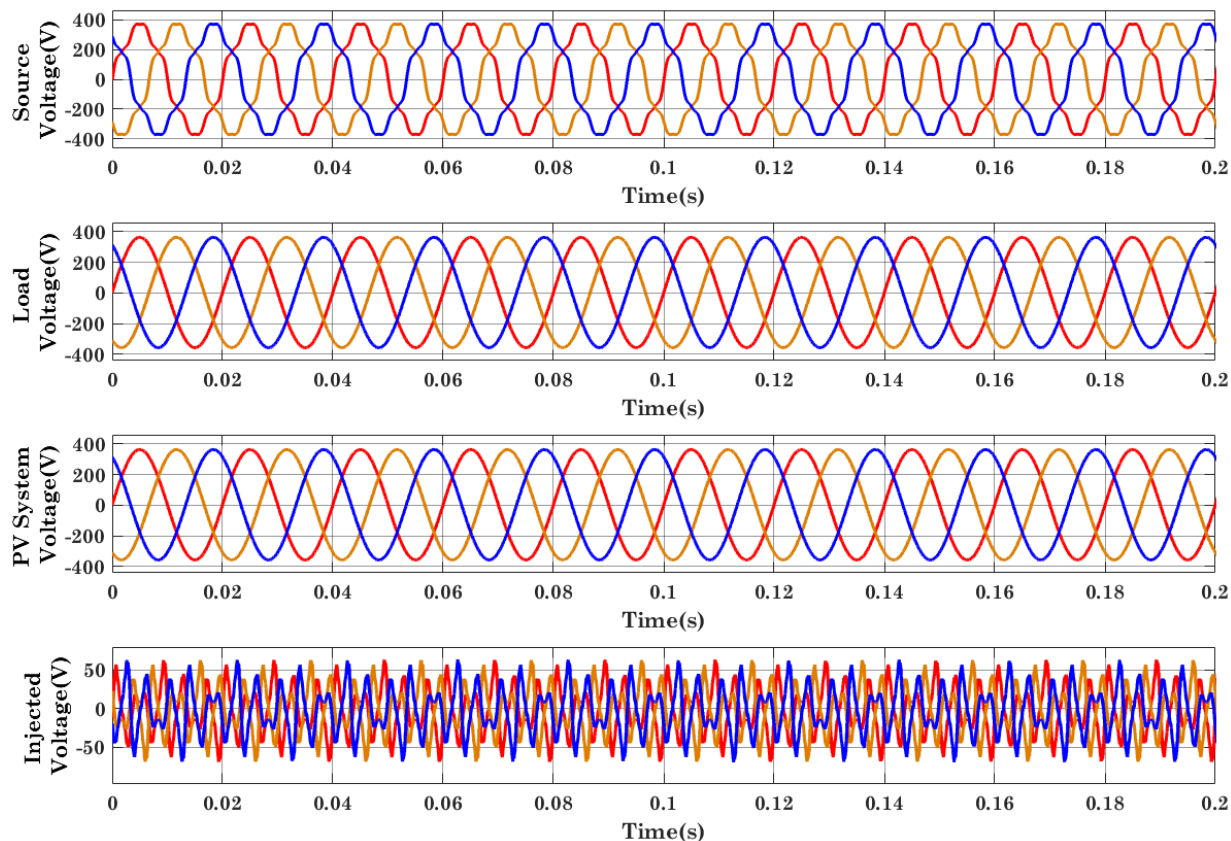


Fig. 13. Source Voltage, Load Voltage, PV System Voltage and Injected Voltage by series converter with proposed ANFIS controlled MMC-UPQC

Figure 14 presents the Load Current, Source Current, PV System Current, and Injected Current by the shunt converter when using the proposed ANFIS-based MMC-UPQC. With the injected current from the shunt converter, the THD of the source current is significantly reduced from 63.47% to 1.05%.

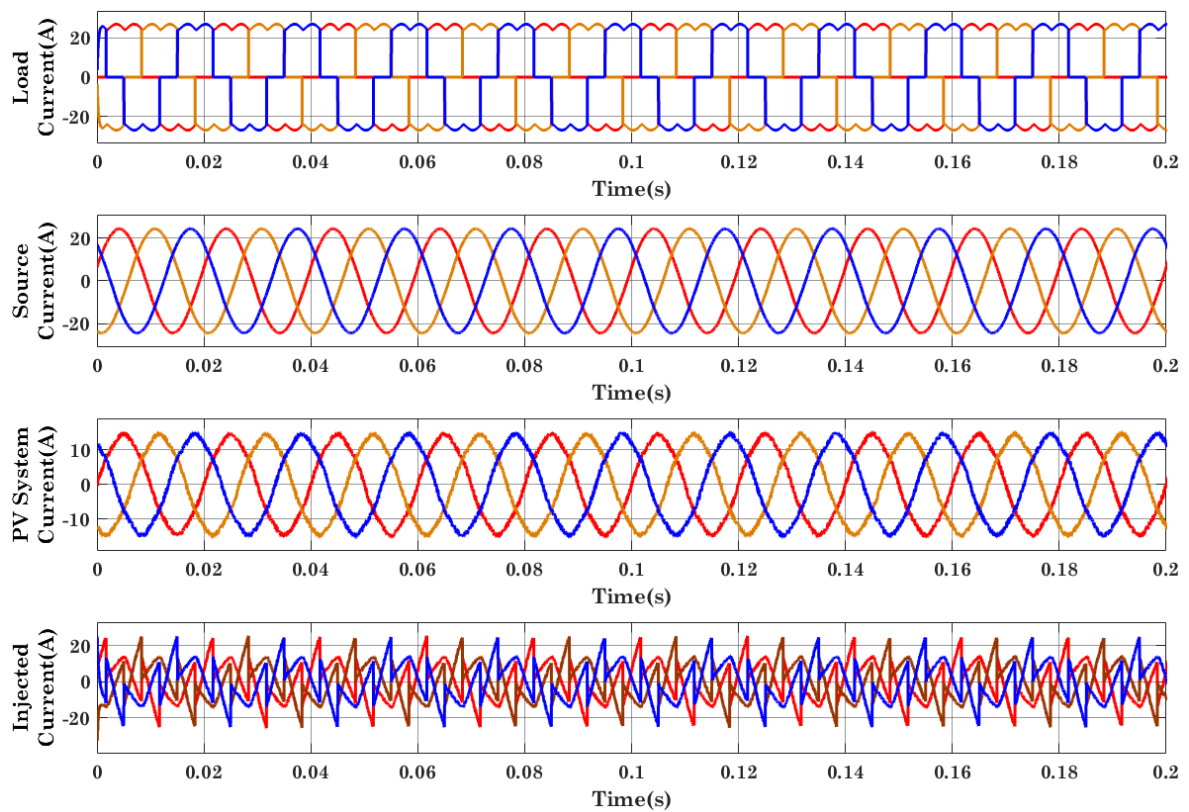


Fig. 14. Load Current, Source Current, PV system current and Injected Current by shunt converter with proposed ANFIS controlled MMC-UPQC

The active power supplied by the grid and PV system to the load, with the implementation of the MMC-UPQC, is shown in Figure 15.

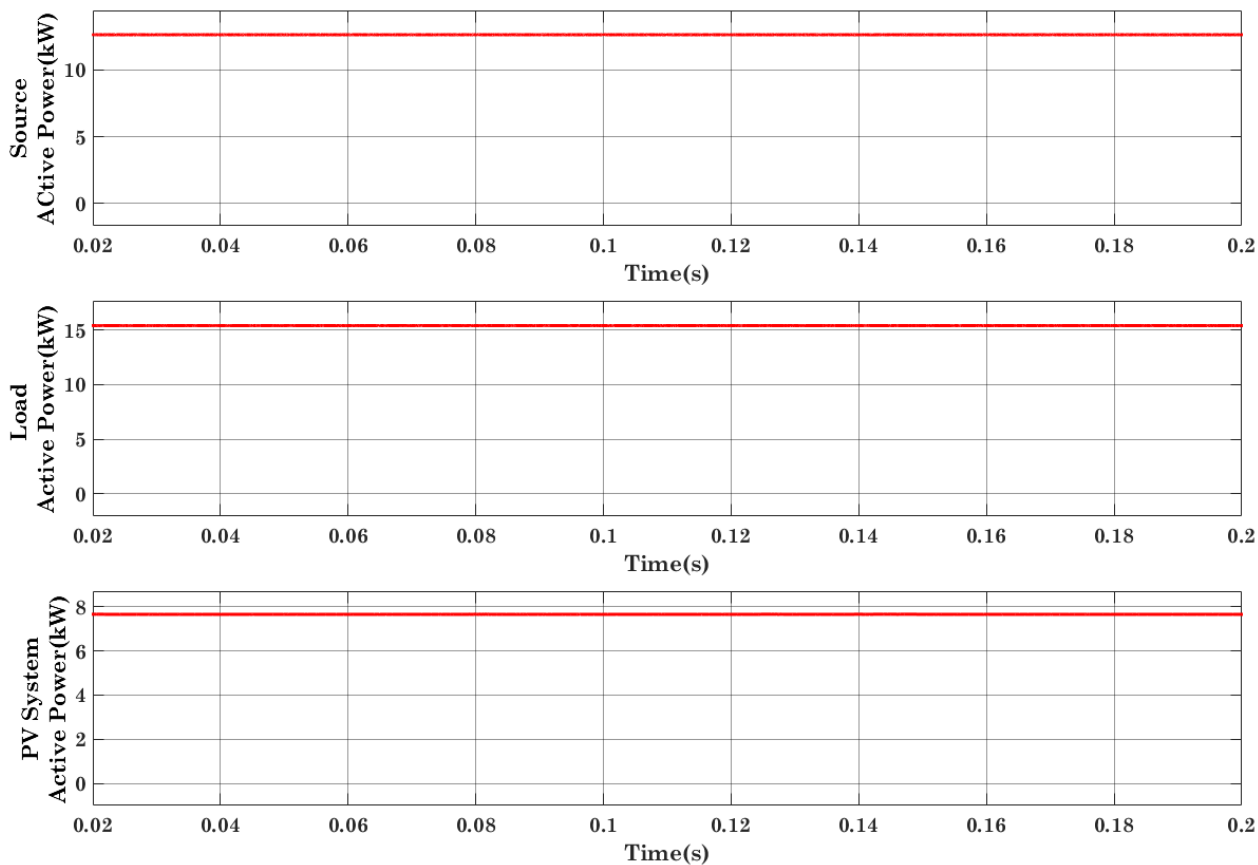


Fig. 15. Instantaneous Active Power at Source, Load and PV System with proposed ANFIS controlled MMC-UPQC

Figures 16 and 19 demonstrate the effectiveness of the ANFIS control approach in maintaining the DC link voltage at the desired reference value of 400V.

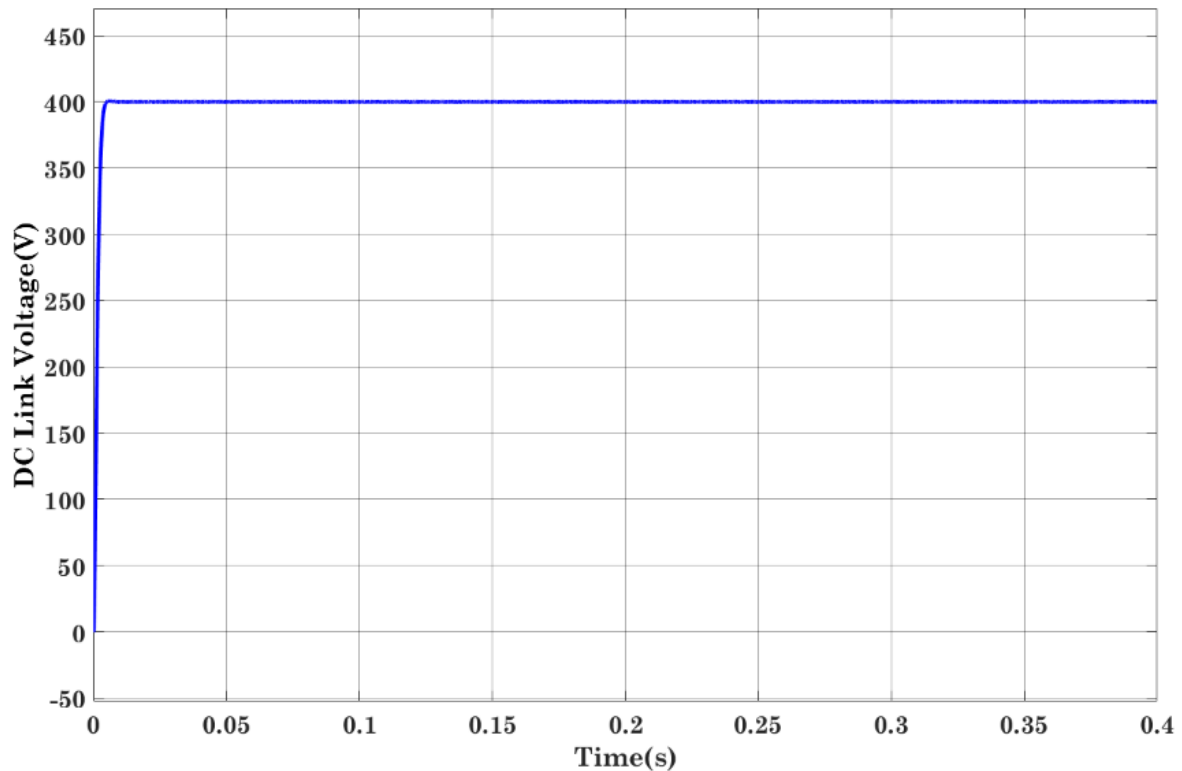


Fig. 16. DC link Voltage with proposed ANFIS controlled MMC-UPQC

Meanwhile, Figures 17 and 18 exhibit the improved compensation performance achieved by the ANFIS-controlled MMC-UPQC. FFT analysis confirms that the ANFIS-controlled MMC-UPQC successfully eliminates harmonics, resulting in a significant reduction in the THD of the load voltage and grid current from 11.62% to 0.63% and from 63.47% to 1.05%, respectively.

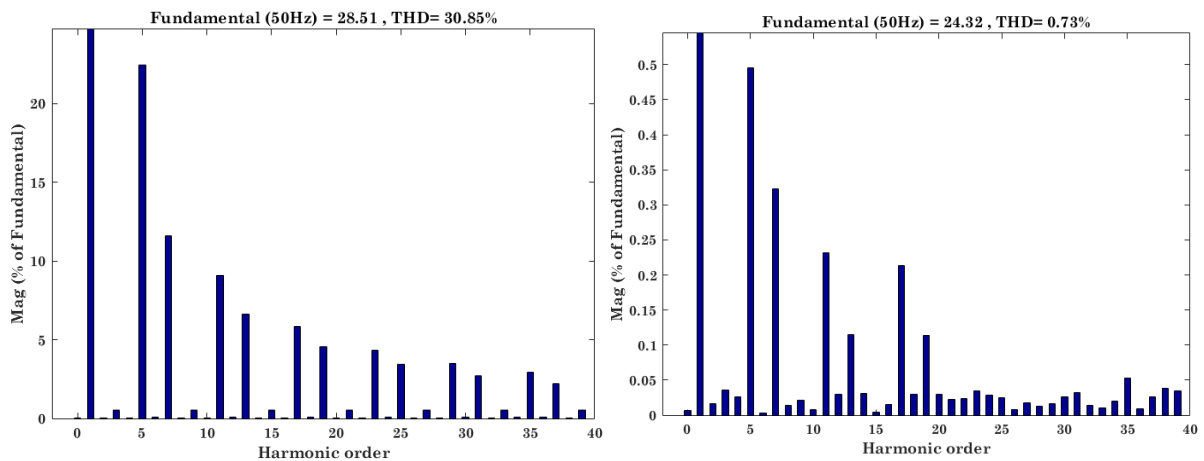


Fig. 17. Load Current and Source Current THD with proposed ANFIS controlled MMC-UPQC

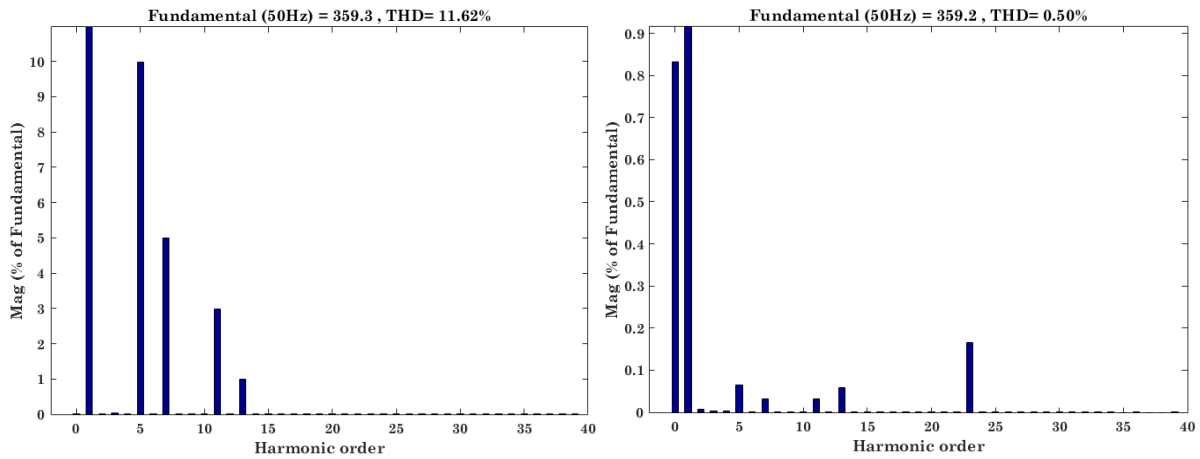


Fig. 18. Source Voltage and Load Voltage THD with proposed ANFIS controlled MMC-UPQC

Furthermore, Figure 19 provides a comparison between the PI-controlled MMC-UPQC, fuzzy-controlled MMC-UPQC, and ANFIS-controlled MMC-UPQC, showcasing the superior performance of the proposed ANFIS control strategy in regulating the DC link voltage under various dynamic conditions.

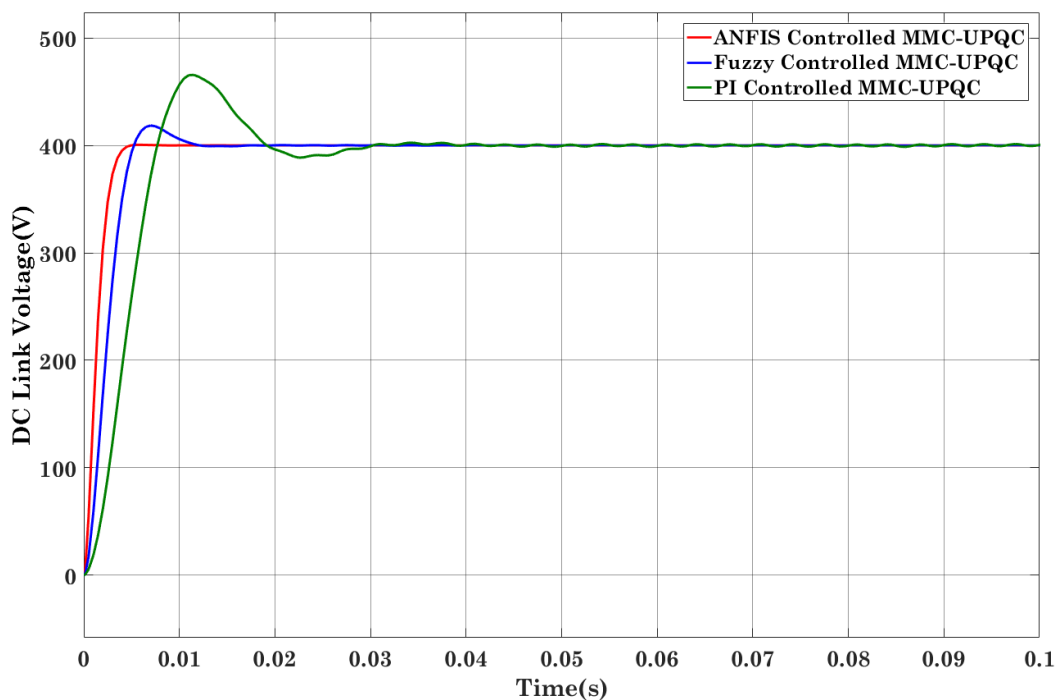


Fig. 19. DC Link Voltage Comparison between PI controlled MMC-UPQC, Fuzzy controlled MMC-UPQC and proposed ANFIS controlled MMC-UPQC

5.2 Case 2: Source Voltage Sag and Swell

This case study focuses on simulating voltage sag and voltage swell conditions using unbalanced grid voltages, considering a pure resistive load. The simulations are conducted to evaluate the performance of the ANFIS-controlled MMC-based UPQC under these challenging conditions. To simulate balanced and unbalanced voltage sag conditions, distorted grid voltages are introduced with a balanced sag of 50% from 0.4 seconds to 0.5 seconds, followed by a sag of 40% on phase A, 30% on phase B, and 20% on phase C after 0.5 seconds. Similarly, to simulate balanced and unbalanced

voltage swell conditions, distorted grid voltages are introduced with a balanced swell of 50% from 0.4 seconds to 0.5 seconds, and a swell of 60% on phase A, 30% on phase B, and 40% on phase C after 0.5 seconds. The evaluation of the ANFIS-controlled MMC-UPQC under sag and swell conditions is depicted in Figures 20 and 21 respectively.

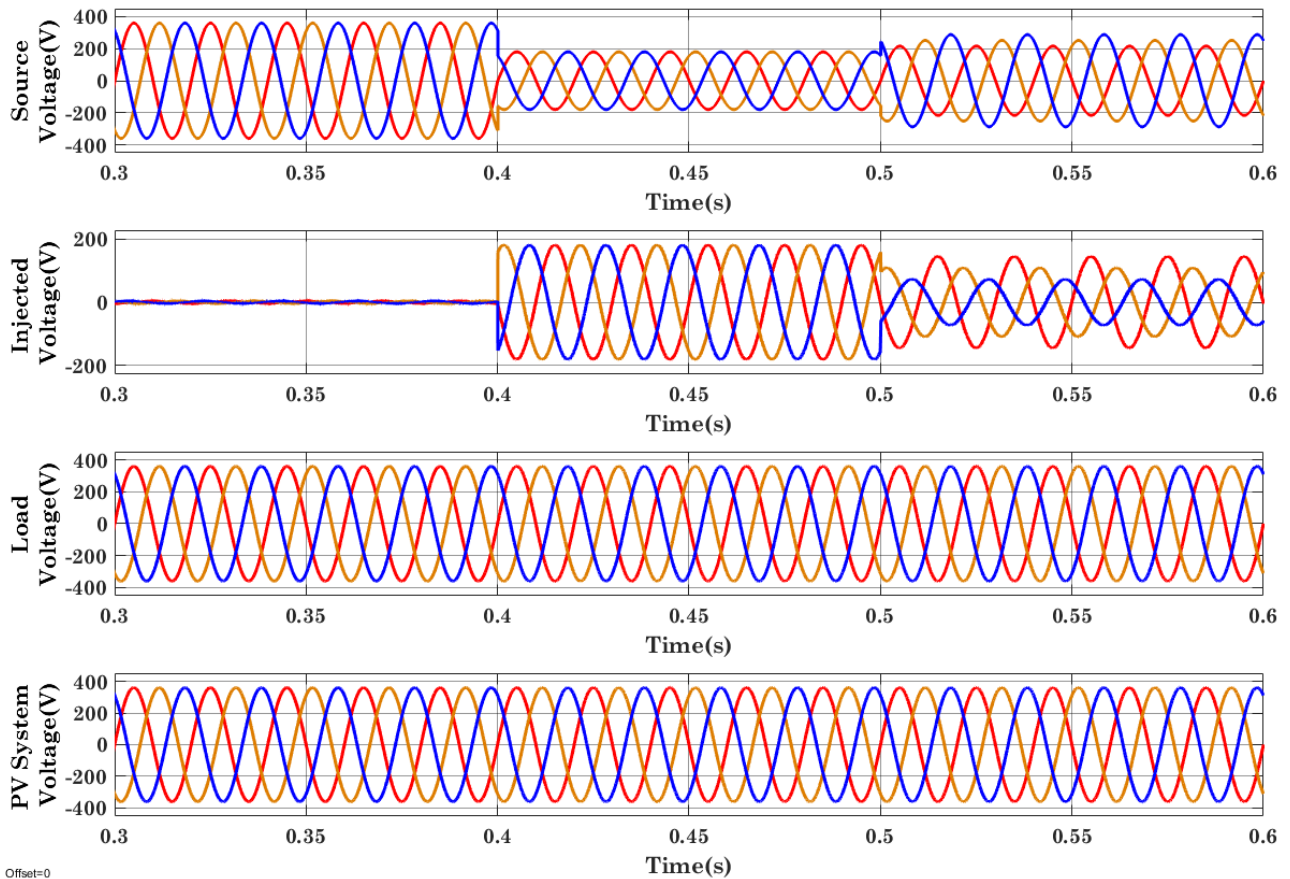


Fig. 20. Source Voltage, Injected Voltage, Load Voltage and PV system Voltage during sag condition with proposed ANFIS controlled MMC-UPQC

The simulation results demonstrate the effectiveness of the ANFIS-controlled MMC-UPQC in compensating for the voltage sag/swell conditions by introducing compensating voltages. These compensating voltages promptly regulate and balance the load voltages to their rated values. Consequently, the system's performance, including the source voltage, load voltage, injected voltage, and DC link voltage, is significantly improved under both sag and swell conditions. The graphs corresponding to the simulation results validate the regulator's ability to maintain stable load voltages despite the severe voltage disturbances. Additionally, the DC link voltage is well-regulated at the reference value of 400V, with a maximum overshoot of 2% within 1 cycle. These findings confirm the MMC-UPQC's capability to sustain load voltage under challenging voltage sag/swell conditions, thereby enhancing the overall stability and performance of the system.

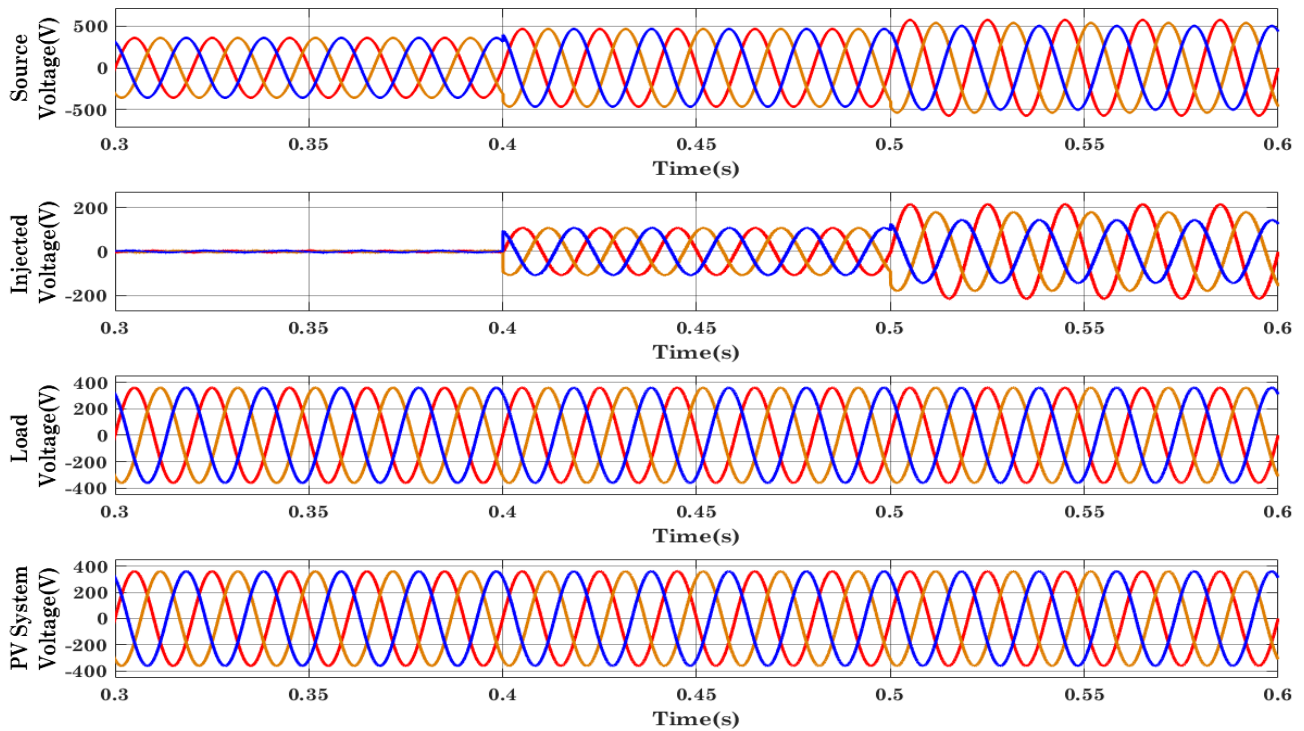


Fig. 21. Source Voltage, Injected Voltage, Load Voltage and PV system Voltage during swell condition with proposed ANFIS controlled MMC-UPQC

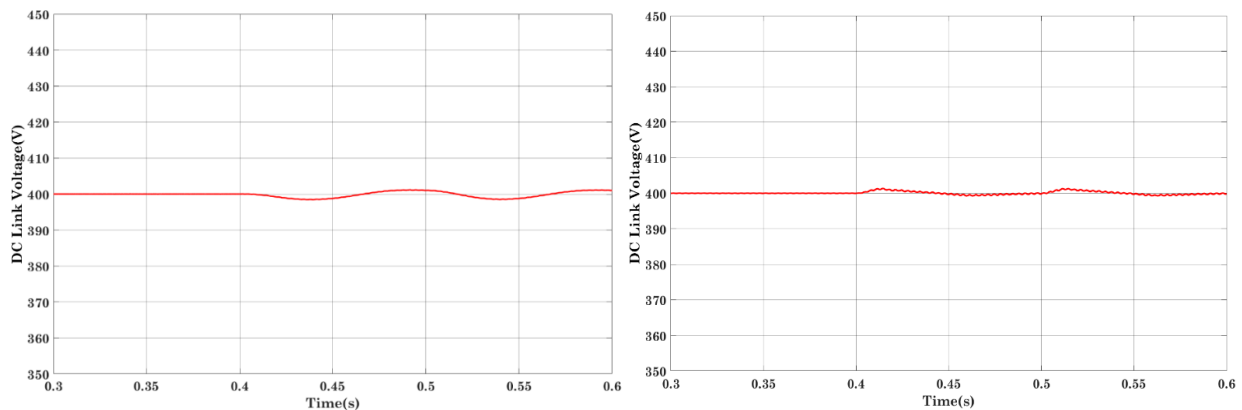


Fig. 22. DC Link Voltage during sag condition and swell condition with proposed ANFIS controlled MMC-UPQC

5.3 Case 3: Distorted Source Voltages and Non-Linear Load

The primary objective of this case study is to assess the dynamic response of the ANFIS-controlled MMC-based UPQC under challenging conditions, particularly in the presence of harmonic grid voltages and increasing nonlinear load. At 0.4 and 0.5 seconds, the nonlinear load is increased, resulting in a corresponding rise in load current, as illustrated in Figure 23.

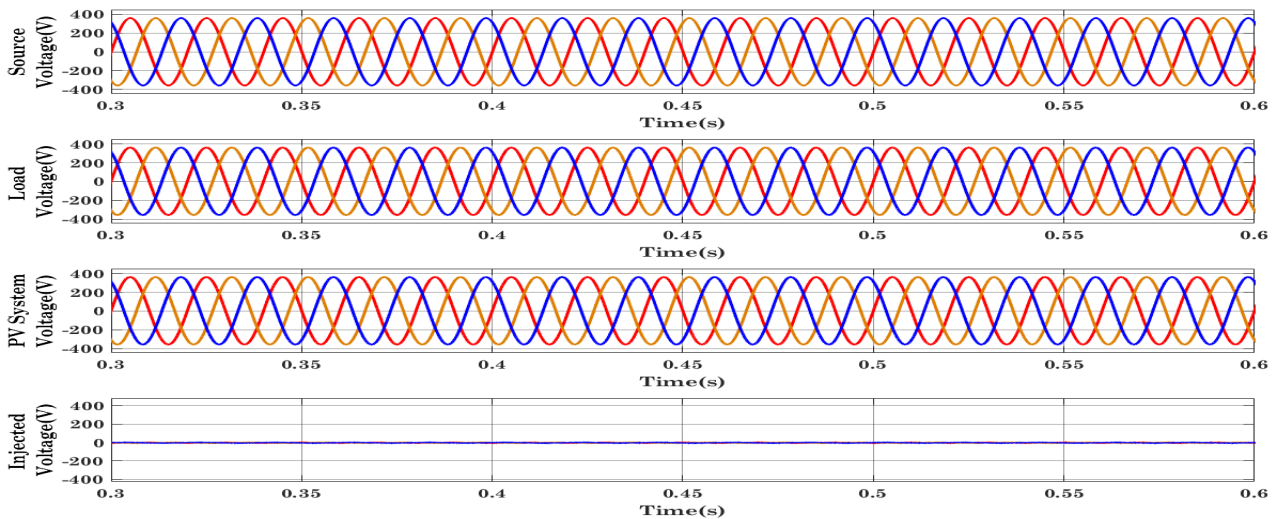


Fig. 23. Source Voltage, Injected Voltage, PV system Voltage and Load Voltage during load increase case with proposed ANFIS controlled MMC-UPQC

Meanwhile, the PV system current remains constant as the input irradiation and temperature of the PV array remain unchanged. The additional power required by the load is sourced from the grid, leading to an increase in source current, as depicted in Figure 24. The shunt converter contributes to reducing the Total Harmonic Distortion (THD) of the source current. Notably, despite the growing active power demand from the load, the ANFIS-controlled MMC-UPQC effectively mitigates harmonics in the output voltages and currents, indicating its competence in handling abrupt load variations.

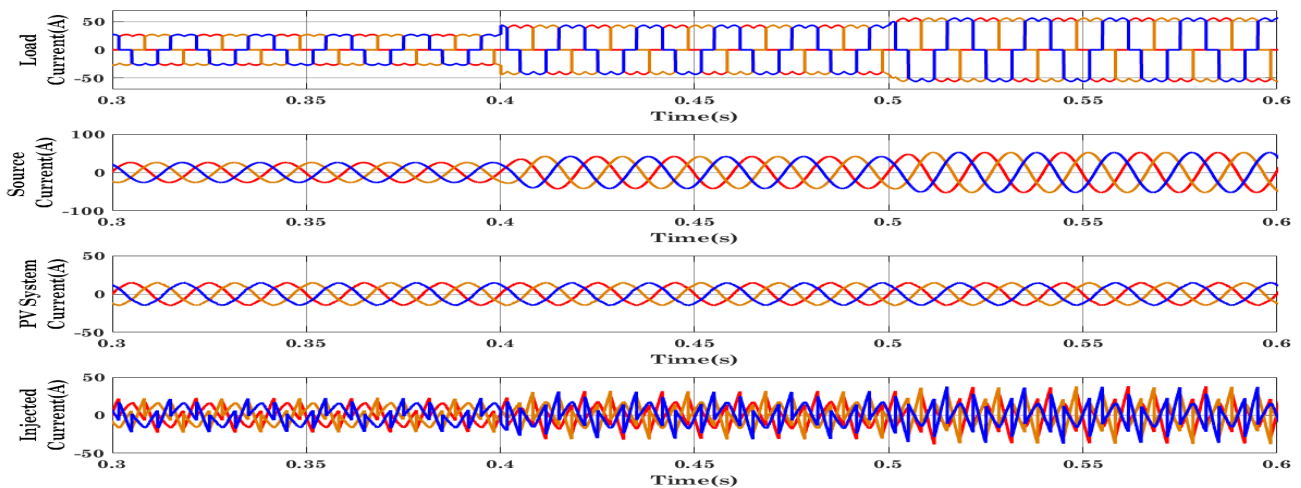


Fig. 24. Load Current, Source Current, PV system Current and Injected Current during load increase case with Proposed ANFIS controlled MMC-UPQC

The dynamic response of the ANFIS-controlled MMC-UPQC under such rapid load changes is thoroughly examined, and the results demonstrate its successful operation even in demanding scenarios involving harmonic, unbalanced, and sag grid voltages. Specifically, at 0.4 seconds, the introduction of a resistive load results in an increase in load current amplitudes. Despite the elevated load active power, the MMC-UPQC maintains stable output voltages and currents. Negligible ripples are observed in the grid current and DC-link voltage, with a maximum overshoot of 1% and a response time of 1 cycle, respectively. These observations indicate the efficient handling of sudden load changes by the ANFIS-controlled MMC-UPQC. Throughout the simulation, the DC-link voltage

remains stable, affirming the MMC-UPQC's ability to sustain excellent compensation performance even in the presence of load variations. This ensures a smooth transition between different operating conditions, further validating the effectiveness of the system. For a constant irradiance $1000\text{W}/\text{m}^2$ active power generated from the PV system is shown in Figure 25(c). Since the load is variable, the active power required by the load, which increases during load changes, is illustrated in Figure 25(b). The grid supplies the additional active power needed by the load, apart from the active power generated by the PV system, as shown in Figure 25(a).

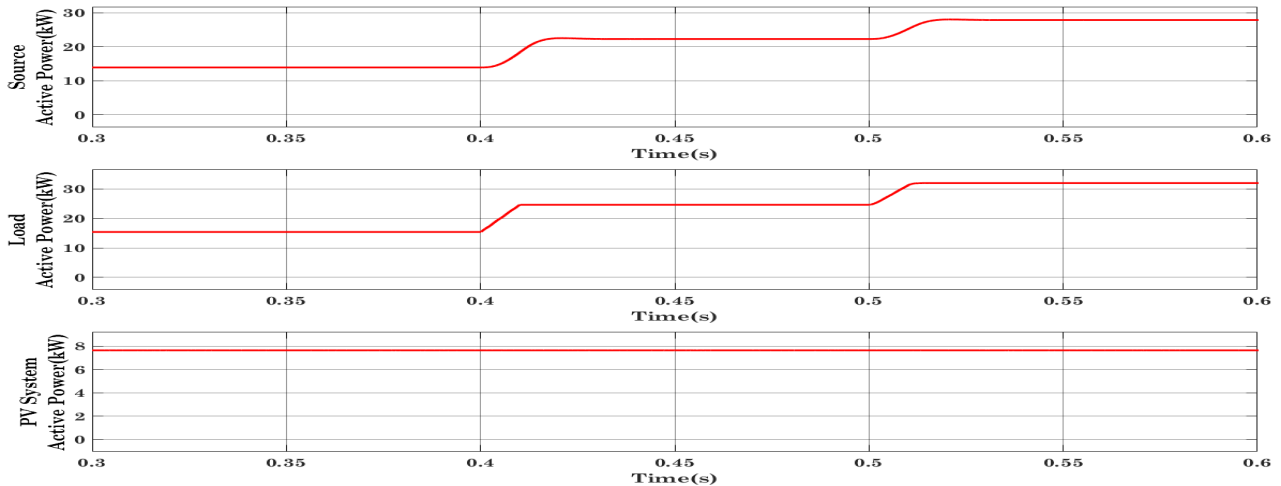


Fig. 25. Instantaneous Active Power at Source, Load and PV System during load increase case with proposed ANFIS controlled MMC-UPQC

5.4 Case 4: Irradiance Change in PV Generating System

In this case response of ANFIS based MMC-UPQC is analysed for different irradiances in PV system. Figure 26 depicts the variation of irradiance which is considered as the input to the PV generation system. As shown in Figure 26, irradiance is reduced from $1000\text{W}/\text{m}^2$ to $400\text{W}/\text{m}^2$ at 0.5 seconds, then increased to $600\text{W}/\text{m}^2$ at 1 second, to $800\text{W}/\text{m}^2$ at 1.5 seconds at last increased to $1000\text{W}/\text{m}^2$ at 2 seconds. A constant non-linear load is connected to the system where the active and reactive power demands of the load are supplied by both PV system and the grid.

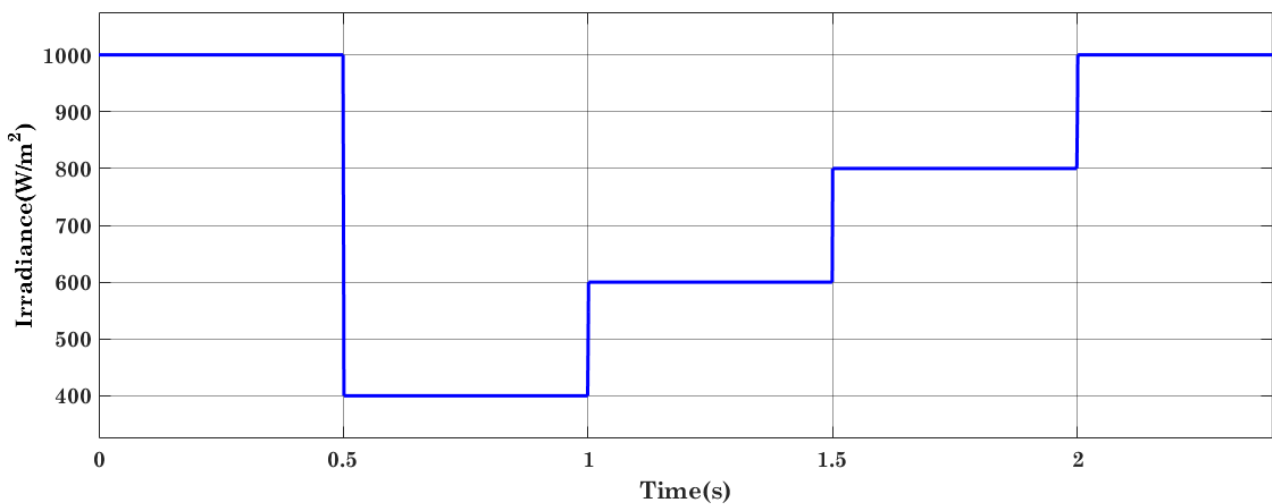


Fig. 26. Irradiance (W/m^2)

Figure 27 illustrates the load current, source current, PV current, and injected current by the shunt converter of the UPQC in response to varying levels of irradiance changes. The THD of the load current is measured at 30.91%, while the THD of the PV system current is found to be 11.62%. However, due to the injected current from the shunt converter of the proposed UPQC, the THD of the source current is significantly reduced to a much lower value of 1.78%.

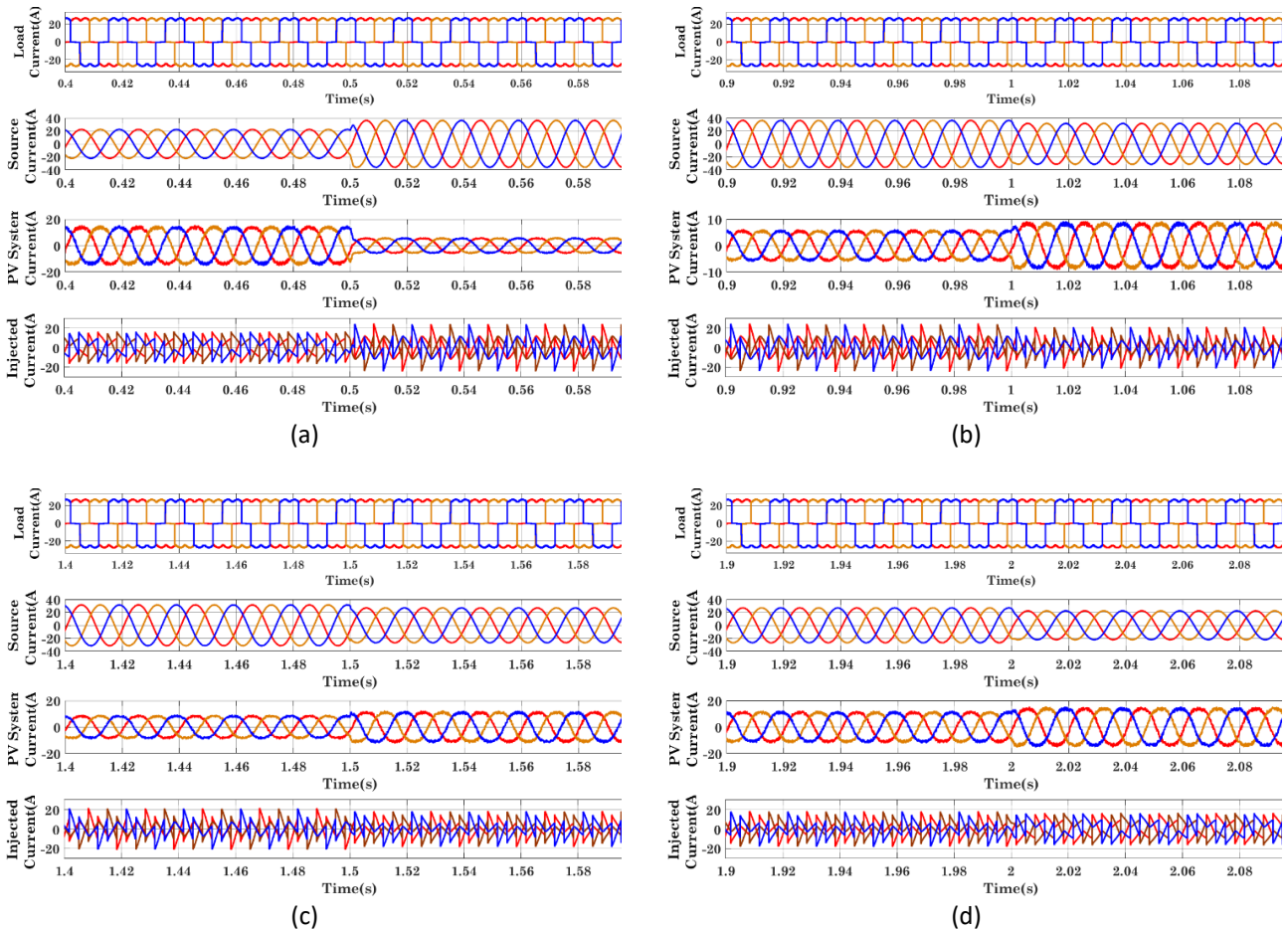


Fig. 27. Load Current, Source Current, PV system Current and Injected Current during load increase case with Proposed ANFIS controlled MMC-UPQC during Irradiance change from (a) 1000 to 400 W/m² (b) 400 to 600 W/m² (c) 600 to 800 W/m² (d) 800 to 1000 W/m²

Figure 28 depicts the power demand of the load, the power generated by the PV generation system, and the power supplied by the grid. If the PV system does not meet the complete power requirement of the load, the additional power needed is sourced from the grid.

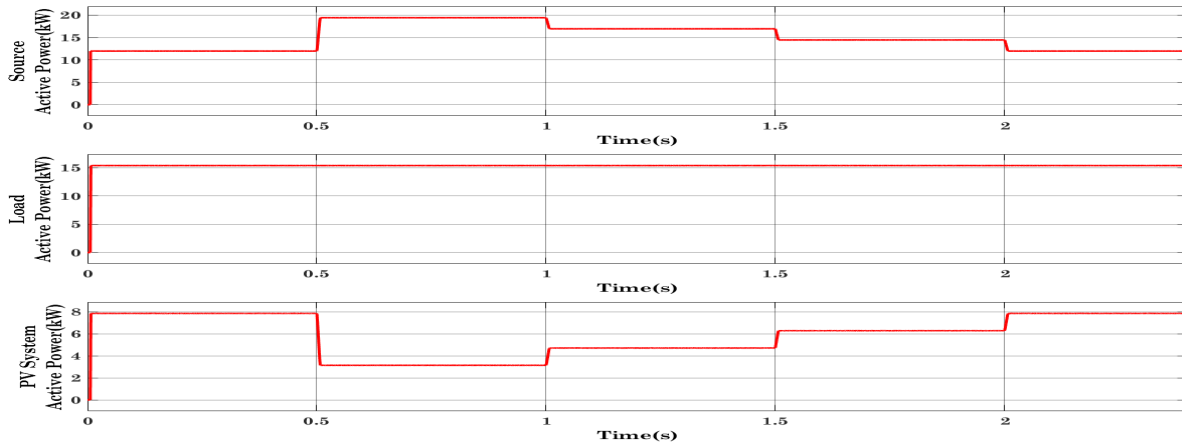


Fig. 28. Instantaneous Active Power at Source, Load and PV System during Irradiance Change with proposed ANFIS controlled MMC-UPQC

5.5 Case 5: Uninterruptible Supply to Load

In this case, real-time variations of irradiance values for a 24-hour period were incorporated, and the system was simulated for a duration of 2.4 seconds using these irradiance values. The variation of irradiance is illustrated in Figure 28.

Figure 29 displays the load current, source current, PV system current, and injected current by the shunt converter of the UPQC.

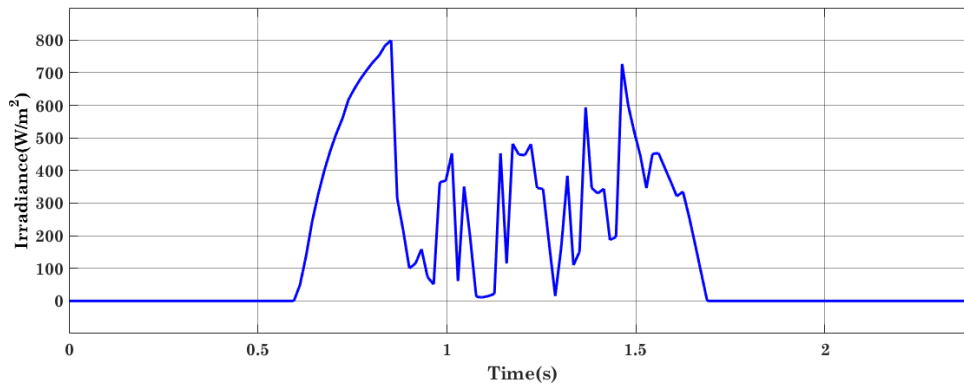


Fig. 29. Irradiance (W/m²)

Load active power, PV active power, and grid active power can be observed in Figure 30.

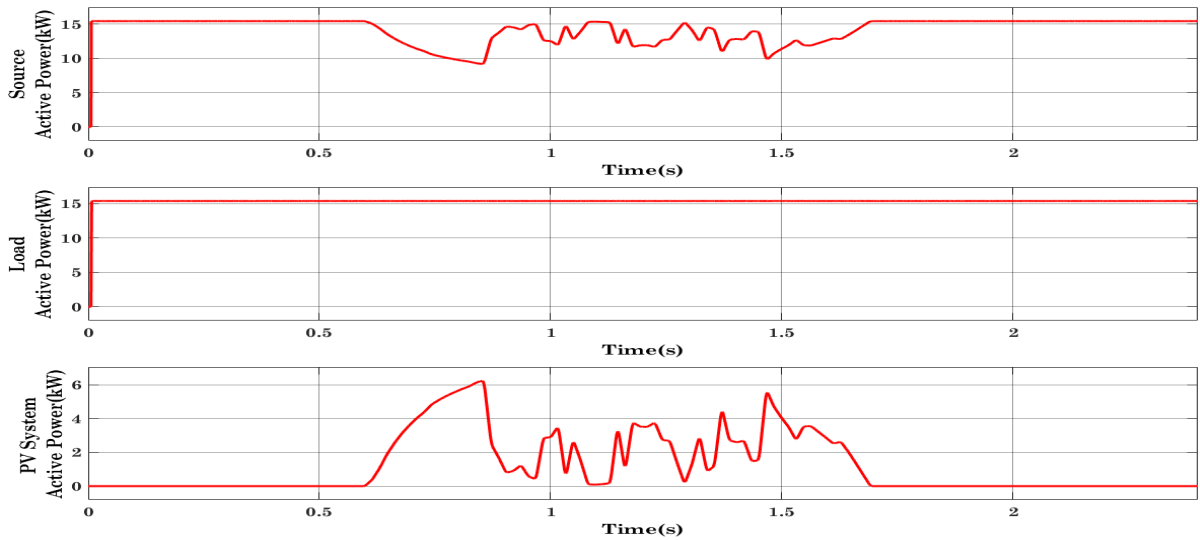


Fig. 30. Instantaneous Active Power at Source, Load and PV System during Irradiance Change with proposed ANFIS controlled MMC-UPQC

5.6 Case 6: PI Controlled MMC-UPQC

In this case Under grid unbalanced MMC-UPQC can deal with the formation of ever more complex grid disturbances. Figure 31 and Figure 32 a passivity-based control (PBC) alongside sliding mode control (SMC) is presented for MMC-UPQC to enhance power quality in power systems with unbalanced grid voltage and controller can increase control precision.

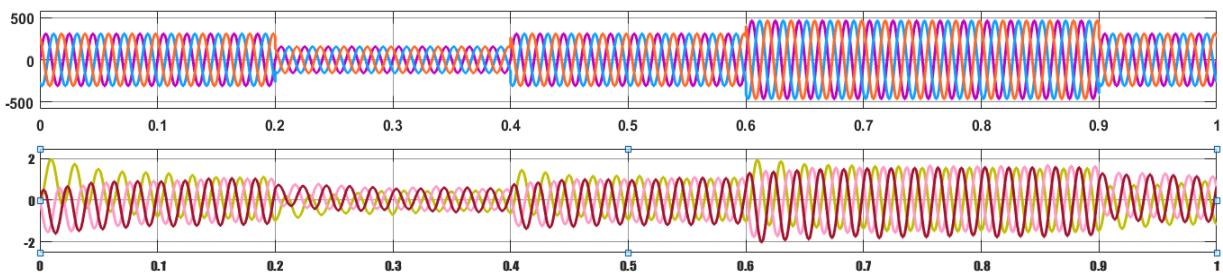


Fig. 31. Source voltage and Current PI Controlled MMC-UPQC

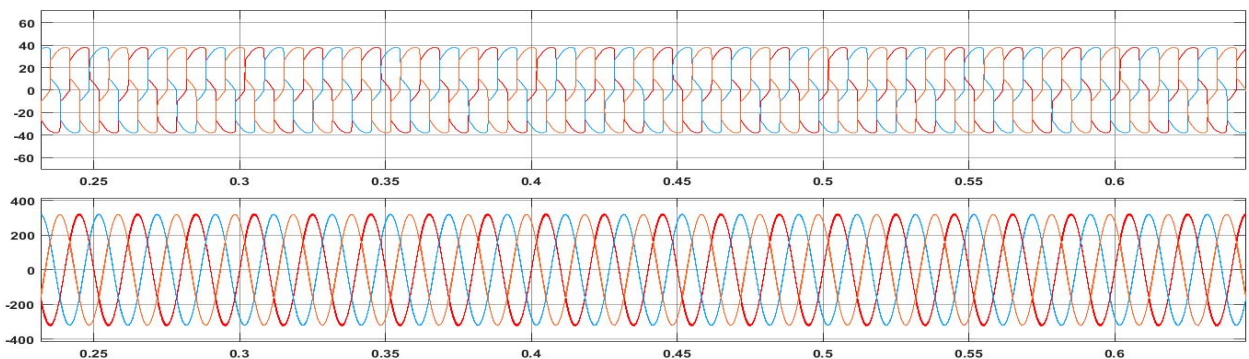


Fig. 32. Load voltage and Current PI Controlled MMC-UPQC

Table 3

Comparison between PI controlled MMC-UPQC, Fuzzy controlled MMC-UPQC and ANFIS controlled MMC-UPQC

	PI controlled MMC-UPQC	Fuzzy controlled MMC-UPQC	ANFIS controlled MMC-UPQC
Source Voltage THD	11.62%	11.62%	11.62%
Load Voltage THD	2.95%	1.52%	0.63%
Load Current THD	30.85%	30.85%	30.85%
Source Current THD	4.85%	2.24%	1.05%
DC Voltage Ripples	0.95%	0.1%	0.06%
Settling Time	0.06 sec	0.0176 sec	0.0085 sec

Figure 33 shows the THD output of source voltage and load of THD output impacted when the power grid voltage swells and sags briefly. As an outcome, recovering the harmonic current in the event of transient swell and sag is critical. Furthermore, PBC demands accurate parameters in the model, whereas in calculated, system characteristics (such as system resistivity) fluctuate with duration.

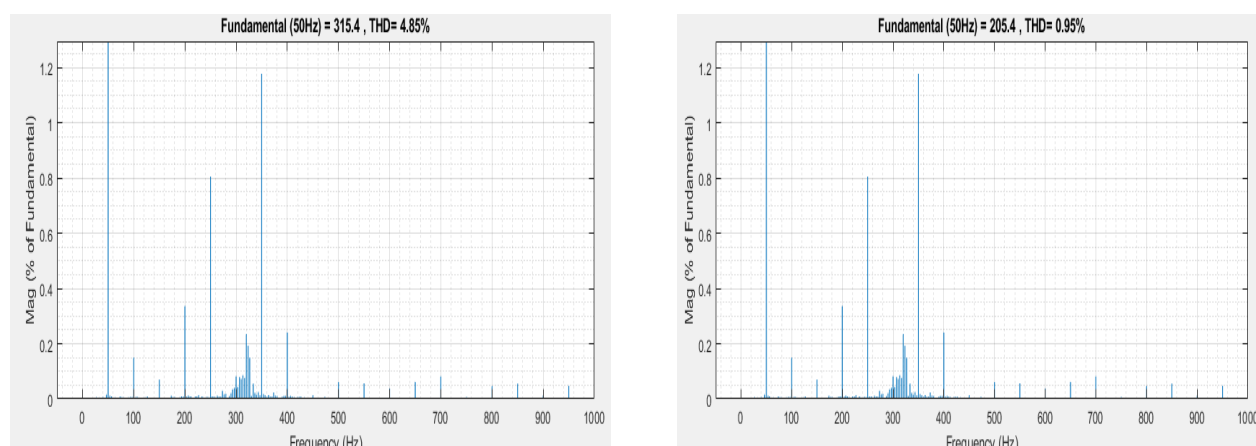


Fig. 33. Source voltage and Load voltage Current THD with PI Controlled MMC-UPQC

6. Conclusion

This novel approach by implementing a Modular Multilevel Converter (MMC) based Unified Power Quality Conditioner (UPQC) within a grid-integrated Photovoltaic (PV) system. Through the integration of an Adaptive Neuro-Fuzzy Inference System (ANFIS) controlled DC link, the MMC-based UPQC exhibits remarkable enhancements in power quality. The effectiveness of this approach lies in its comprehensive control strategies applied to both the shunt Harmonic Active Power Filter (HAPF) and the series Active Power Filter (APF) components of the UPQC. The shunt HAPF employs a dual-loop feedback mechanism along with a voltage feedforward approach to effectively counteract harmonic currents and simultaneously maintain the stability of the DC-link voltage. Meanwhile, the series APF relies on a voltage feedback mechanism combined with a current feedforward technique to regulate distorted load voltage. An innovative pre-sorting Sliding-Mode Generalized Discrete Fourier Transform (SGDFT) method, based on the Sequential Resonant Filter (SRF) Phase-Locked Loop (PLL) concept, is proposed. This SGDFT-pre-filter significantly enhances the resilience of the SRF-PLL, enabling reliable operation even under abnormal grid voltage conditions. The proposed ANFIS controller for MMC-based UPQC excels in multiple aspects, including the successful regulation of DC voltage, effective mitigation of voltage and current harmonics originating from the PV system's

Voltage Source Converter (VSC), and the compensation of reactive power fluctuations. Simulation outcomes convincingly showcase the superiority of the ANFIS controller over conventional Proportional Integral (PI) and fuzzy controllers, affirming its ability to markedly improve power quality. By accurately suppressing voltage and current harmonics, the UPQC not only ensures enhanced power quality but also contributes to the stability of grid operations. The significance of this capability underscores the utility of employing the ANFIS-controlled MMC-based UPQC within grid-connected PV systems. It provides a robust solution for the mitigation of disturbances and harmonics originating from the PV system's VSC, ultimately promoting a cleaner and more reliable power supply. To advance this promising strategy, further research and practical experimentation are recommended to validate its efficacy in real-world scenarios and to optimize its performance.

Acknowledgement

This research was not funded by any grant.

References

- [1] Hernández-Callejo, Luis, Sara Gallardo-Saavedra, and Víctor Alonso-Gómez. "A review of photovoltaic systems: Design, operation and maintenance." *Solar Energy* 188 (2019): 426-440. <https://doi.org/10.1016/j.solener.2019.06.017>
- [2] Yin, Shuo, Xing Chen, Zhe Chai, Man Jin, Youxin Sang, and Yibo Li. "A Power Quality Pricing Method Considering Resonance in Electricity Retail Market." In *2021 IEEE 5th Conference on Energy Internet and Energy System Integration (EI2)*, pp. 3512-3517. IEEE, 2021. <https://doi.org/10.1109/EI252483.2021.9713473>
- [3] Nadine, Kaza Ikuzwe, and Peter Musau Moses. "Grid-connected solar PV with Active Power Filter Services for Power Quality Improvement." In *2022 IEEE PES/IAS PowerAfrica*, pp. 1-5. IEEE, 2022. <https://doi.org/10.1109/PowerAfrica53997.2022.9905276>
- [4] Fahim, Abrar, Mehedi Hasan, and Muhtasim Alam Chowdhury. "Smart parking systems: comprehensive review based on various aspects." *Heliyon* 7, no. 5 (2021). <https://doi.org/10.1016/j.heliyon.2021.e07050>
- [5] Irechukwu, Michael E., and Aviti T. Mushi. "Proposal for Single Wire Earth Return Distribution System for Homboza Village Electrification." *International Journal of Mechatronics, Electrical and Computer Technology (IJMEC)* 11, no. 39 (2021): 4837-4842.
- [6] Rastegar, Farzad, and Zohreh Paydar. "Improving the Performance of Unified Power Quality Conditioner Using Interval Type 2 Fuzzy Control." In *2022 30th International Conference on Electrical Engineering (ICEE)*, pp. 437-441. IEEE, 2022. <https://doi.org/10.1109/ICEE55646.2022.9827396>
- [7] Guo, Qi, Fan Xiao, Chunming Tu, Fei Jiang, Rongwu Zhu, Jian Ye, and Jiayuan Gao. "An overview of series-connected power electronic converter with function extension strategies in the context of high-penetration of power electronics and renewables." *Renewable and Sustainable Energy Reviews* 156 (2022): 111934. <https://doi.org/10.1016/j.rser.2021.111934>
- [8] Huang, Han, L. Zhang, O. J. K. Oghorada, and Mingxuan Mao. "A delta-connected MMCC-based active power conditioner for unbalanced load compensation and harmonic elimination." *International Journal of Electrical Power & Energy Systems* 118 (2020): 105811. <https://doi.org/10.1016/j.ijepes.2019.105811>
- [9] Diaz, Matias, Roberto Cárdenas Dobson, Efrain Ibaceta, Andrés Mora, Matias Urrutia, Mauricio Espinoza, Felix Rojas, and Patrick Wheeler. "An overview of applications of the modular multilevel matrix converter." *Energies* 13, no. 21 (2020): 5546. <https://doi.org/10.3390/en13215546>
- [10] Golla, Mallikarjuna, S. Thangavel, Sishaj Pulikottil Simon, and Narayana Prasad Padhy. "An enhancement of power quality with efficient active power transfer capability in a PV-BSS-fed UAPF for microgrid realization." *IEEE Systems Journal* 17, no. 1 (2022): 1614-1625. <https://doi.org/10.1109/JSYST.2022.3179182>
- [11] Liu, Hong, Rongrong Ji, Jie Li, Baochang Zhang, Yue Gao, Yongjian Wu, and Feiyue Huang. "Universal adversarial perturbation via prior driven uncertainty approximation." In *Proceedings of the IEEE/CVF International Conference on Computer Vision*, pp. 2941-2949. 2019. <https://doi.org/10.1109/ICCV.2019.00303>
- [12] Xie, Wei. "Applying analysis of power quality enhancement by using UPQC." In *IOP Conference Series: Earth and Environmental Science*, vol. 371, no. 5, p. 052010. IOP Publishing, 2019. <https://doi.org/10.1088/1755-1315/371/5/052010>
- [13] Rezaei, Mohammad Amin, Majid Nayeripour, Jiefeng Hu, Shahab S. Band, Amir Mosavi, and Mohammad-Hassan Khooban. "A new hybrid cascaded switched-capacitor reduced switch multilevel inverter for renewable sources and domestic loads." *IEEE access* 10 (2022): 14157-14183. <https://doi.org/10.1109/ACCESS.2022.3146256>

- [14] Hans, Florian, Walter Schumacher, Shih-Feng Chou, and Xiongfei Wang. "Design of multifrequency proportional–resonant current controllers for voltage-source converters." *IEEE Transactions on Power Electronics* 35, no. 12 (2020): 13573-13589. <https://doi.org/10.1109/TPEL.2020.2993163>
- [15] Voutsas, Venetia, Demian Battaglia, Louise J. Bracken, Andrea Brovelli, Julia Costescu, Mario Diaz Munoz, Brian D. Fath *et al.*, "Two classes of functional connectivity in dynamical processes in networks." *Journal of the Royal Society Interface* 18, no. 183 (2021): 20210486. <https://doi.org/10.1098/rsif.2021.0486>
- [16] Tavakoli, Parisa, Nima Vaezi, Parastou Fahim, and Ali Karimpour. "A New Approach Based on Fuzzy-Adaptive Structure & Parameter Learning Applied in Meta-Cognitive Algorithm for ANFIS." In *2021 7th international conference on control, instrumentation and automation (ICCIA)*, pp. 1-5. IEEE, 2021. <https://doi.org/10.1109/ICCIA52082.2021.9403539>
- [17] Bai, Kaiyuan, Xiaomin Zhu, Shiping Wen, Runtong Zhang, and Wenyu Zhang. "Broad learning based dynamic fuzzy inference system with adaptive structure and interpretable fuzzy rules." *IEEE Transactions on Fuzzy Systems* 30, no. 8 (2021): 3270-3283. <https://doi.org/10.1109/TFUZZ.2021.3112222>
- [18] Ehteram, Mohammad, Fang Yenn Teo, Ali Najah Ahmed, Sarmad Dashti Latif, Yuk Feng Huang, Osama Abozweita, Nadhir Al-Ansari, and Ahmed El-Shafie. "Performance improvement for infiltration rate prediction using hybridized adaptive neuro-fuzzy inferences system (ANFIS) with optimization algorithms." *Ain Shams Engineering Journal* 12, no. 2 (2021): 1665-1676. <https://doi.org/10.1016/j.asej.2020.08.019>
- [19] Claudino, Daniel, Jerimiah Wright, Alexander J. McCaskey, and Travis S. Humble. "Benchmarking adaptive variational quantum eigensolvers." *Frontiers in Chemistry* 8 (2020): 606863. <https://doi.org/10.3389/fchem.2020.606863>
- [20] Can, Özer, Tolga Baklacioglu, Erkan Öztürk, and Onder Turan. "Artificial neural networks modeling of combustion parameters for a diesel engine fueled with biodiesel fuel." *Energy* 247 (2022): 123473. <https://doi.org/10.1016/j.energy.2022.123473>